

26  
27  
28  
29  
30  
31  
32  
33  
34  
35  
36  
37  
38  
39  
40  
41  
42  
43  
44  
45  
46  
47  
48  
49  
50

**Performance of AIRS ozone retrieval over the central Himalayas: Case studies of biomass burning, downward ozone transport and radiative forcing using long-term observations**

Prajwal Rawat<sup>1,5</sup>, Manish Naja<sup>1</sup>, Evan Fishbein<sup>2</sup>, Pradeep K. Thapliyal<sup>3</sup>, Rajesh Kumar<sup>4</sup>, Piyush Bhardwaj<sup>4</sup>, Aditya Jaiswal<sup>1</sup>, Sugriva N. Tiwari<sup>5</sup>, Sethuraman Venkataramani<sup>6</sup>, Shyam Lal<sup>6</sup>

<sup>1</sup> Aryabhata Research Institute of Observational Sciences (ARIES), Nainital, 263001, India

<sup>2</sup> NASA Jet Propulsion Laboratory, Pasadena, CA 91109, USA

<sup>3</sup> Space Applications Centre, ISRO, Ahmedabad 380015, India

<sup>4</sup> National Center for Atmospheric Research (NCAR) Boulder, CO 80307, USA

<sup>5</sup> DDU Gorakhpur University, Gorakhpur 273009, India

<sup>6</sup> Physical Research Laboratory (PRL), Ahmedabad, 380009, India

**Corresponding author:** Manish Naja ([manish@aries.res.in](mailto:manish@aries.res.in))

77

**78 Short Summary:**

79 Satellite based ozone observations have gained wide importance due to their global coverage.

80 However, satellite retrieved products are indirect and need to be validated, particularly over

81 mountains. Here, ozonesondes launched from a Himalayan site are utilized to assess the AIRS

82 ozone retrieval. AIRS is shown to overestimate ozone in the upper troposphere and lower

83 stratosphere, while the differences with ozonesonde are lower in the middle troposphere and

84 middle stratosphere.

85

86

87

88

89

90

91

92

93

94

95

96

97

98

99

100

101

102

## 134 Abstract

135 Data from 242 ozonesondes launched from ARIES Nainital (29.40° N, 79.50° E, and 1793 m  
136 elevation) are used to evaluate the Atmospheric Infrared Sounder (AIRS) version 6 ozone profiles  
137 and total column ozone during the period 2011-2017 over the central Himalaya. The AIRS ozone  
138 products are analyzed in terms of retrieval sensitivity, retrieval biases/errors, and ability to retrieve  
139 the natural variability of columnar ozone, which has not been done so far from the Himalayan  
140 region having complex topography. For a direct comparison, averaging kernels information is used  
141 to account for the sensitivity difference between the AIRS and ozonesonde data. We show that  
142 AIRS has lower ~~differences-difference~~ with ozonesonde in the lower and middle troposphere and  
143 stratosphere with nominal underestimations of less than 20%. However, in the upper troposphere  
144 and lower stratosphere (UTLS), we observe a considerable overestimation of the magnitude, as  
145 high as 102%. The weighted statistical error analysis of AIRS ozone shows higher positive bias  
146 and standard deviation in the upper troposphere of about 65% and 25%, respectively. Similar to  
147 AIRS, Infrared Atmospheric Sounding Interferometer (IASI) and Cross-track Infrared Sounder  
148 (CrIS) are also able to produce ozone ~~peakspeak~~ altitudes and gradients successfully. However,  
149 the statistical errors are again higher in the UTLS region that are likely related to larger variability  
150 of ozone, lower ozone partial pressure and inadequate retrieval information on the surface  
151 parameters. Furthermore, AIRS fails to capture the monthly variation of the total ozone column,  
152 with a strong bimodal variation, unlike unimodal variation seen in ozonesonde and Ozone  
153 Monitoring Instrument (OMI). In contrast, the UTLS and ~~the~~ tropospheric ozone ~~column~~ columns  
154 are in reasonable agreement. Increases in ~~the~~ ozone ~~of values by 5 - 20% (in 2 - 6 km altitude)~~ after  
155 ~~the~~ biomass burning and during events of downward transport ~~(in 2 - 16 km altitude)~~ are captured  
156 well by AIRS. Ozone radiative forcing (RF) derived from total column ozone using ozonesondes  
157 data (4.86 mW/m<sup>2</sup>) matches well with OMI (4.04 mW/m<sup>2</sup>), while significant RF underestimation  
158 is seen in AIRS (2.96 mW/m<sup>2</sup>). The fragile and complex landscapes of the Himalayas are more  
159 sensitive to global climate change, and establishing such biases and error analysis of space-borne  
160 sensors will help study the long-term trends and estimate accurate radiative budgets.

161

162

163

164

## 1. Introduction

Atmospheric ozone is an essential trace gas that plays a crucial role in the atmospheric oxidizing chemistry, air quality, and earth's radiative budget. The stratospheric ozone absorbs harmful solar ultraviolet radiation and protects biological life on earth, whereas tropospheric ozone, being a secondary air pollutant (Logan et al., 1985; Pitts and Pitts, 1997; Pierce et al., 2009; [Monks et al., 2015](#); [Lelieveld et al., 2018](#)) and greenhouse gas, contributes to global warming and can harm human health and crops when present in higher concentrations near the surface (Fishman et al., 1979; Ebi and McGregor 2008; Lal et al., 2017). Different radiative forcing of ozone from the stratosphere (cooling) to the troposphere (heating) (Lacis et al., 1990; Forster et al., 2007; Wang et al., 1993; Hegglin et al., 2015) demonstrate its potential importance as an atmospheric climate gas (Shindell et al., 2012); [Thornhill et al., 2021](#)). Hence, information regarding precise long-term variability in global ozone distribution is vital for better characterizing atmospheric chemistry and global climate changes (McPeters et al., 1994; Kim et al., 1996; [Myhre et al., 2017](#)).

In recent decades, observations of ozone from space-borne sensors (microwave limb sounding, UV-VIS, and IR) have become an increasingly robust tool for global and higher temporal monitoring (Fishman et al., 1986; Munro et al., 1998; Bhartia et al., 1996; Foret et al., 2014). This increases our ability to analyze various influences of human activities on the atmospheric chemical composition, including ozone, study their long-term impact on climate (Fishman et al., ~~1987~~, [1987](#); [Fry et al., 2012](#); [Tarasick et al., 2019](#); [Thornhill et al., 2021](#)), and estimate reliable radiative budgets (Hauglustaine and Brasseur 2001; Gauss et al., 2003; Aghedo et al., 2011). However, the space-based sensors are indirect and measure the atmospheric composition based upon specific algorithms utilizing radiative transfer models and a-priori information. Hence, the

234 retrieval outputs need to be evaluated with certain reference instruments for establishing the  
235 credibility and better utilization of space-borne data.

236  
237 The Himalayas, a complex terrain region, has the largest abundance of ice sheets outside polar  
238 regions that impacts global/regional radiative budgets and climate pervasively (e.g., Lawrence and  
239 Lelieveld, ~~2010; Lelieveld2010; Cristofanelli et al., 2014; Zhang et al., 2015).~~ Very sparse 2018).  
240 ~~Here, the in-situ and ground-based observations are very sparse and limited, and complex~~  
241 ~~topography in this region,~~ along with inadequate information on the surface parameters ~~make,~~  
242 makes it difficult to retrieve atmospheric composition from space-borne instruments. This is  
243 because the ozone weighting function, a measure of the retrieval sensitivity and a fundamental  
244 retrieval component, depends upon various atmospheric parameters like surface temperature,  
245 surface emissivity, and terrain height (Rodgers et al., 1976, 1990; Bai et al., 2014), which is not  
246 uniform over the foot-print size of the AIRS (~ 13 km x 13 km) over the Himalayas. Usually, the  
247 ozone weighting function has a shorter integrating path over the elevated terrain regions, which  
248 follows a smaller weighting function and provides lesser sensitivity and higher errors in the final  
249 retrievals (Coheur et al., 2005; Bai et al., 2014). ~~Apart from the terrain height, retrieval also~~  
250 ~~depends on other factors like surface emissivity, atmospheric input constituents, input error~~  
251 ~~minimizing parameters, etc., whose accuracy matters, alters the retrieval processes abruptly, and~~  
252 ~~introduces error in the final retrieval.~~

253  
254 The Atmospheric Infrared Sounder (AIRS) onboard the Aqua satellite has been providing reliable  
255 vertical profiles of ozone, temperature, water vapor, and other trace gases globally twice a day  
256 since 2002. Numerous validation studies of AIRS retrieved ozone have been carried out for

280 different versions since it started operating (2002). For example, Bian et al. (2007) studied AIRS  
281 version 4 over Beijing and discussed the potential agreements (within 10%) between AIRS and  
282 ozonesonde (GPSO3) ozone, particularly in the upper troposphere and lower stratosphere (UTLS)  
283 region with the capability of AIRS to identify various Stratosphere-Troposphere Exchange (STE)  
284 and transient convective events. Similarly, a study over Boulder and Lauder by Monahan et al.  
285 (2007) using a similar AIRS version showed despite the larger biases in the lower and middle  
286 tropospheric region, the retrieval algorithm captures the ozone variability very effectively with a  
287 positive correlation of more than 70%. However, that study suggested a need for tropopause-  
288 adjusted coordinates in the a-priori profiles. Both these studies (Bian et al., 2007; Monahan et al.,  
289 2007) show larger biases of AIRS ozone in the lower and middle tropospheric regions; however,  
290 shifts in retrieval biases and errors were seen towards the UTLS region in version 5 (Divakarla et  
291 al., 2008), apart from significant improvements in the lower troposphere. The retrieval  
292 methodology has also changed significantly between V4 and V5. Version 4 or earlier used  
293 regression retrieval as the first guess in physical retrieval, while later versions used a climatology-  
294 based first guess for the physical retrieval based on other works (McPeters et al., 2007). Also,  
295 radiative transfer models, selected channel sets, and clarified quality indicators have been modified  
296 and improved in all successive versions.

297  
298 The AIRS ozone retrieval in V5 has improved significantly with retrieval biases and root mean  
299 square error (RMSE) less than 5% and 20%, respectively (Divakarla et al., 2008), over the tropical  
300 regions. However, there is not much discussion and studies of the assessment for AIRS ozone over  
301 the Himalayas' complex terrain, where retrieval is expected to be erroneous due to large surface  
302 variability within its footprint. Also, most of the previous studies (Bian et al., 2007; Divakarla et

al., 2008; Pittman et al., 2009) did not utilize the averaging kernels information of the AIRS that is vital for satellite evaluation.

328

Here, the evaluation of AIRS version 6, which entirely depends upon the infra-red (IR) observations after the failure of the AMSU sensor, is presented in terms of statistical analysis and ability to retrieve the natural variability of ozone at various altitudes over the central Himalayan region using in-situ ozonesonde observations convolved with AIRS averaging kernels. Additionally, the present study assessed the AIRS retrieval algorithm using IASI and CrIS radiance information for one year. AIRS columnar ozone (i.e., total, UTLS, and tropospheric columns) is also assessed with ozonesonde, OMI, and Microwave Limb Sounder (MLS) observations. AIRS has a long-term data set for ozone and meteorological parameters, establishing such biases and error analysis is essential to make meaningful use of its data to characterize the Himalayan atmosphere, study the trends, radiative budgets, perform the model evaluation and data assimilation over this region.

340

## 341 **2 Data and Methodology**

### 342 **2.1 Data Description**

#### 343 **2.1.1 AIRS**

344 Atmospheric Infrared Sounder (AIRS) onboard Aqua satellite, in the sun synchronous  
345 sunsynchronous polar orbit at 705 km altitude, is a hyperspectral thermal infrared grating  
346 spectrometer with equatorial crossings at ~13:30 local time (LT). It is a nadir scanning sensor that  
347 was deployed in orbit on May 4, 2002. AIRS, along with its partner microwave instrument, the  
348 Advanced Microwave Sounding Unit (AMSU-A), represents the most advanced atmospheric

372 sounding system placed in space using cutting-edge infrared and microwave technologies. These  
373 instruments together observe the global energy cycles, water cycles, climate variations, and  
374 greenhouse gases, however, after AMSU failure, the retrieval now mostly depends upon the AIRS  
375 IR observations. The AIRS infrared spectrometer acquires 2378 spectral samples at resolutions  
376 ( $\lambda/\Delta\lambda$ ) ranging from 1086 to 1570  $\text{cm}^{-1}$ , in three bands: 3.74  $\mu\text{m}$  to 4.61  $\mu\text{m}$ , 6.20  $\mu\text{m}$  to 8.22  $\mu\text{m}$ ,  
377 and 8.8  $\mu\text{m}$  to 15.4  $\mu\text{m}$  (Fishbein et al., 2003; Pagano et al., 2003). The independent channels of  
378 AIRS permit retrieval of various atmospheric states and constituents depending upon their  
379 corresponding spectral response, even in the presence of a 90% cloud fraction (Susskind et al.,  
380 2003; Maddy and Barnett, 2008). In this study, we have used Level 2 Support physical products of  
381 AIRS (AIRS2SUP). The AIRS2SUP files (~240 granules/day) possess extra information over the  
382 standard AIRS files, e.g., information on averaging kernel and degree of freedom, including  
383 vertical profiles at 100 pressure levels, against just 28 in the standard product.

384  
385 The support product profiles contain 100 levels between 1100 and 0.016 mbar. While it has a  
386 higher vertical resolution, the vertical information content is no greater than the standard product.  
387 The information on averaging kernels and degree of freedoms (DOFs) is utilized to understand the  
388 retrieved products more comprehensively. The DOFs of ozone, a measure of significant eigen  
389 functions used in the AIRS retrieval, ~~has~~ have an average value of 1.36 over the tropical latitude  
390 band (Maddy and Barnett 2008) (Table S1), while over the balloon collocated region, an average  
391 DOFs of 1.62 is observed (Figure S1). In the present study, the AIRS data is flagged as best quality  
392 when the cloud fraction is less than 80%, and the degrees of freedom (DOF) ~~is~~ are greater than  
393 0.04. However, analysis of cloud fraction over our collocated ~~position-region~~ shows (Figure S2)  
394 only 7% of observations during 2011 - 2017 ~~has~~ had a cloud fraction of more than 80%.



418

419

420

### 421 2.1.2 IASI (NOAA/CLASS)

422 The Infrared Atmospheric Sounding Interferometer (IASI) onboard MetOp satellites, with a

423 primary focus on meteorology than climate and atmospheric chemistry monitoring, is a nadir

424 viewing Michelson interferometer (Clerbaux et al., 2007). The first MetOp satellite was launched

425 in October 2006 (MetOp-A), and IASI was declared operational in July 2007. MetOp is a polar

426 sun-synchronous satellite having deseendingdescend and aseendingascend nodes at 09:30 and

427 21:30 LT, respectively. IASI measures in the IR part of the EM spectrum at a horizontal resolution

428 of 12 km at nadir up to 40 km over a swath width of about 2,200 km. IASI covers an infra-red

429 spectral range between 3.7 to 15.4  $\mu\text{m}$  with a total of 8461 spectral channels, out of which 53

430 channels around 9.6  $\mu\text{m}$  are utilized for ozone retrieval. IASI level 2 ozone products provided by

431 NOAA National Environmental Satellite Data and Information Service (NESDIS) Center for

432 Satellite Application and Research (STAR) are used in this study. The IASI (NOAA/CLASS)

433 ozone product is retrieved based on the AIRS algorithm and has various quality control flags

434 (Table S2). Only QC=0 data which represents a successful IR ozone retrieval, is used.

435

### 436 2.1.3 CrIS/ATMS (NUCAPS)

437 The Cross-track Infrared Sounder (CrIS) and Advanced Technology Microwave Sounder (ATMS)

438 onboard the Suomi NPP satellite were launched in 2011 to feature the high spectral-resolution

439 (“hyperspectral”) observations of earth’s atmosphere. The CrIS instrument is an advanced Fourier

440 transform spectrometer with an ascending node 13:30 LT and flies at a mean altitude of 824 km

464 and performs fourteen orbits per day. It measures high-resolution IR spectra in the spectral range  
465 650 - 2550  $\text{cm}^{-1}$  with a total of 1305 channels. The ATMS is a microwave sounder with a total of  
466 22 channels ranging from 23 to 183 GHz. These two instruments, CrIS and ATMS, operate in an  
467 overlapping field-of-view (FOV) formation, with ATMS FOVs re-sampled to match the location  
468 and size of the  $3 \times 3$  CrIS FOVs for retrieval under clear to partly cloudy conditions. Here the  
469 NUCAPS algorithm-based ozone product of CrIS is utilized. The NOAA Unique CrIS/ATMS  
470 Processing System (NUCAPS) is a heritage algorithm developed by the STAR team based on the  
471 AIRS retrieval algorithm (Susskind et al., 2003, 2006). The NOAA implemented NUCAPS  
472 algorithm is a modular architecture that was specifically designed to be compatible with multiple  
473 instruments. The same retrieval algorithms are currently used to process the AIRS/AMSU suite  
474 (operations since 2002), the IASI/AMSU/MHS suite (operational since 2008), and now the  
475 CrIS/ATMS suite (approved for operations in January 2013). Here again, various quality controls  
476 for retrieved data are provided by the NUCAPS science algorithm team, and we used QC=0 for  
477 lesser discrepancies in our evaluation- (Table S2). These research products follow a similar  
478 retrieval algorithm as developed by the AIRS science team, which gives us further opportunity to  
479 assess the AIRS retrieval algorithm for IASI and CrIS radiances.

480

#### 481 **2.1.4 Ozonesonde**

482 Electrochemical concentration cell (ECC) ozonesondes and GPS-radiosondes have been launched  
483 from the Aryabhata Research Institute of Observational Sciences (ARIES) ( $29.4^\circ$  N,  $79.5^\circ$  E, and  
484 1793 m elevation) Nainital (Figure 1), a high-altitude site in central Himalaya, since 2011 (Ojha  
485 et al., 2014; Rawat et al., 2020), the only facility in the Himalayan region having regular  
486 launchings. ECC ozonesonde relies on the oxidation reaction of ozone with potassium iodide (KI)

510 solution (Komhyr et al., 1967, 1995) to measure ozone partial pressure in the ambient atmosphere.  
511 The typical vertical resolution of ozonesonde is about 100 - 150 m and has a precision of better  
512 than  $\pm 3 - 5 \%$  with an accuracy of about  $\pm 5 - 10 \%$  up to 30 km altitude under standard operating  
513 procedures (Smit et al., 2007). The ozonesonde is connected to iMet-radiosonde via a V7 electronic  
514 interface, where radiosonde consists of GPS, PTU, and a transmitter to transmit signals to the  
515 ground. Due to higher accuracy and in-situ measurement, ozonesonde has been widely used  
516 worldwide for satellite and model validation (Divakarla et al., 2008; Nassar et al., 2008; Monahan  
517 et al., 2007; Kumar et al., 2012a, 2012b; Dufour et al., 2012; Verstraeten et al., 2013; Boynard et  
518 al., 2016; Rawat et al., 2020). Both the ascending and descending data were recorded by  
519 ozonesonde, however, due to time lag in descending records, only ascending data is utilized (Lal  
520 et al., 2013, 2014; Ojha et al., 2014). The data is collected at the interval of about 10 meters which  
521 is averaged over 100 meters interval using a  $3\sigma$  filter that removes the outlier values (Srivastava  
522 et al., 2015; Naja et al., 2016).

523

#### 524 **2.1.5 Other Auxiliary Data**

525 Additionally, collocated and concurrent OMI and MLS observations are also used to study the  
526 tropospheric ozone, UTLS, and total ozone column due to their reasonable sensitivity and well-  
527 validated retrievals (Veefkind et al., 2006; Ziemke et al., 2006; Fadnavis et al., 2014; Wang et al.,  
528 2021). The tropospheric ozone column obtained from OMI and MLS is based on the residual  
529 method, which depends upon the collocated difference between the MLS stratospheric ozone  
530 column and OMI total ozone column, which is described in ~~details-detail~~ by Ziemke et al. (2006).  
531 Furthermore, the MLS version 4 data is utilized for the UTLS column above 261 hPa due to its  
532 credibility in this range for scientific applications (Livesey et al., 2013; Schwartz et al., 2015).

556 Moreover, for fair statistical analysis between ozonesonde and MLS ozone profile, ~~a~~-Gaussian  
557 smoothing is applied to ozonesonde with full width at half maximum ~~equals equal~~ to typical upper  
558 tropospheric vertical resolution ( $\sim 2 - 4$  km) of MLS (Livesey et al., 2013). The best quality data  
559 of MLS with data flags, i.e., status=even, quality > 0.6, and convergence < 1.18, is utilized (Ziemke  
560 et al., 1998; Barre et al., 2012) ~~is used~~. However, a slightly different collocation criterion of  $3^\circ \times 3^\circ$   
561 grid box and daytime collocation is utilized for MLS in this work, due to coarser resolution and to  
562 get sufficient matchups.

563

## 564 2.2 Methods of Analysis

565 The balloon launch time is mostly around 12:00 IST (Indian Standard Time, which is 5.5 hours  
566 ahead of GMT). The Aqua satellite comes over the ~~Indian region~~India around 1:30 pm and 1:30  
567 am IST. Hence for collocation, only noontime (ascending) data (or  $\pm 3$  hours of balloon launch)  
568 with  $1^\circ \times 1^\circ$  spatial collocation were chosen in this evaluation. However, for some days, there was  
569 no noontime granule in AIRS retrieval (nearly 35 out of total 242 soundings), then we used ~~a~~ loose  
570 collocation of  $\pm 1$  day. However, no significant changes were seen after such flexible collocation.  
571 Most of the ozonesondes have burst altitudes near 10 hPa, hence AIRS ozone profiles are evaluated  
572 from surface to 10 hPa.

573

574 Although suitable collocation criteria have been defined for a fair comparison, still different  
575 vertical resolutions of the two data sets (ozonesonde  $\sim 100$  m and AIRS  $\sim 1-5$  km) make the  
576 meaningful comparison difficult (~~Smit et al., 2007~~; Maddy and Barnet, 2008; ~~Verstraeten et al.,~~  
577 ~~2013~~; ~~Boynard et al., 2016~~). The difference in vertical resolution and retrieval sensitivity ~~has~~  
578 ~~to~~must be accounted for a meaningful comparison. Though there is no perfect way to remove the

601 error arising from the different vertical resolutions of the two measurements, still utilizing the  
 602 averaging kernel smoothing or Gaussian smoothing, the error is minimized. Various groups have  
 603 used the satellite averaging kernels smoothing to compare satellite measurements with ozonesonde  
 604 (Zhang et al., 2010; Verstraeten et al., 2013; Boynard et al., 2016, 2018), while Gaussian  
 605 smoothing (Wang et al., 2020) and broad layer columns (Nalli et al., 2017) are also utilized. In the  
 606 present analysis, averaging kernel smoothing is utilized. First, ozonesonde data were interpolated  
 607 at all AIRS Radiative Transfer Algorithm (RTA) layers from surface to burst altitude, then  
 608 ozonesonde profiles ~~are~~were smoothed according to the AIRS averaging kernel and a-priori  
 609 profile (ML climatology), leading to a vertical profile [ozonesonde (AK)] representing what AIRS  
 610 would have measured for the same ozonesonde sampled atmospheric air mass in the absence of  
 611 any other error affecting satellite observations. According to Rodgers and Connor (2003), the  
 612 smoothing of the true state can be characterized as follows:

$$613 \quad X_{\text{est}} = X_0 + A'(X_{\text{sonde}} - X_0) \quad (1)$$

614 The AIRS provides averaging kernels information at 9 pressure levels (Figure 2b) whereas the  
 615 AIRS RTA has 100 pressure levels. So following ozone vertices (Table S3) and formulating  
 616 trapezoid matrix (Figure 2a, the details regarding the calculation of trapezoid matrices are given  
 617 in AIRS/AMSU/HSB Version 6 Level 2 Product Levels, Layers and Trapezoids), we convert 9  
 618 levels AIRS averaging kernels to 100 levels averaging kernels using following defined operation.

$$619 \quad A' = F \times A_{\text{trapezoid}} \times F' \quad (2)$$

620 Where  $A_{\text{trapezoid}}$  and  $F$  are averaging kernel matrices and trapezoid matrices ( $F'$  is pseudo-inverse  
 621 of  $F$ ).  $A_{\text{trapezoid}}$  is a given product, while  $F$  is calculated for given ozone vertices (Table S3).

622

645 Further, in the thermal IR spectrum, the contribution of ozone or any other trace gas towards  
 646 emission/absorption of IR radiation in the radiative transfer equation depends on the exponent of  
 647 layer integrated column amounts (Maddy and Barnett, 2008). Hence logarithmic changes in layer  
 648 column density are more linear than absolute changes. So logarithmic equations are used instead  
 649 of ~~eq~~Eq. 1 for smoothing ozonesonde data in the present study.

$$\ln (X_{\text{est}}) = \ln (X_0) + A' \{ \ln (X_{\text{sonde}}) - \ln (X_0) \} \quad (3)$$

651 Where  $X_{\text{est}}$ ,  $X_{\text{sonde}}$ , and  $X_0$  are smooth ozonesonde or ozonesonde (AK), true ozonesonde, and first  
 652 guess (ML climatology) profiles, respectively.

653 More details on the calculation of averaging kernels can be found in AIRS documents  
 654 (AIRS/AMSU/HSB Version 6 Level 2 Product Levels, Layers and Trapezoids) or in available  
 655 literature (Maddy and Barnett, 2008; Irion et al., 2018). A typical averaging kernels matrix and  
 656 other parameters are shown in Figure 2. ~~Here~~ Figure 2a shows a typical trapezoid matrix, Figure  
 657 2b shows the averaging kernels at 9 pressure levels, Figure 2c shows constructed averaging kernels  
 658 at 100 RTA layers, and Figure 2d shows an example ~~for~~ of the different ozone profiles convolved  
 659 with AKs on 15 June 2011 over the observation site.

660

### 661 2.3 Statistical Analysis

662 The error analysis for AIRS retrieval with interpolated and smoothed ozonesonde is based on Nalli  
 663 et al. (2013, 2017). Bias, root mean squared error (RMSE), and standard deviation (STD) are  
 664 studied at various RTA vertical levels from the surface to 10hPa over the Himalayan region. The  
 665 finer spatio-temporal collocation utilized here has further minimized the uncertainty and error in  
 666 the evaluation. Since the observation site (29.4° N, 79.5° E) is at a latitude lower than 45°; hence

688 there is a lesser overlap of satellite passes, and mostly a few nadir scans are close to the observation  
 689 site (mostly daytime granules in the range of 75 to 85). Hence all the daytime observations of  
 690 AIRS are close to  $\pm 3$  hours of temporal collocation to the ozonesonde launch and possess a lesser  
 691 chance of time mismatch.

692  
 693 Given the collocated ozone mixing ratio profiles for satellite, ozonesonde (AK), and insitu-in-situ  
 694 truth (ozonesonde) observations, the statistical errors are calculated as follows -

695  
 696 
$$\text{RMSE} (\Delta O_l) = \sqrt{\frac{\sum_{j=1}^{j=n} W_{l,j} \times (\Delta O_{l,j})^2}{\sum_{j=1}^{j=n} W_{l,j}}} \quad (4)$$

697  
 698 
$$\text{Bias} (\Delta O_l) = \frac{\sum_{j=1}^{j=n} W_{l,j} \times (\Delta O_{l,j})}{\sum_{j=1}^{j=n} W_{l,j}} \quad (5)$$

699 Here  $l$  runs over different RTA layers and  $j$  runs for all collocated profiles,  $\Delta O_{l,j}$  the fractional  
 700 deviation is taken to be the absolute deviation divided by the observed value.

701 Where  $\Delta O_{l,j} = \left( \frac{O^R_{l,j} - O^T_{l,j}}{O^T_{l,j}} \right)$ , ~~where~~  $O^T$  and  $O^R$  are ozonesonde/ozonesonde (AK) and satellite  
 702 retrieved ozone mixing ratio, respectively.

703  $W_{l,j}$  is the weighting factor and assumes one of three forms  $W_0 = 1$ ,  $W_1 = O^R$  and  $W_2 = (O^R)^2$  and  
 704 for ozone to minimize skewing impact due to large variation in mixing ratio at different altitudes,  
 705 we have used the  $W_2$  weight factor as suggested by other sounder science team (Nalli et al., 2013,  
 706 2017).

707 The Standard deviation (STD) is then calculated as follows

708

$$STD(\Delta O_3) = \sqrt{[RMSE(\Delta O_3)]^2 - [Bias(\Delta O_3)]^2} \quad (6)$$

by the square root of difference between RMSE and biases square at different RTA levels. Further to check the strength of the linear relationship between the satellites retrieved data and ozonesonde data the square of Pearson’s correlation coefficient is also calculated as follows.

$$r = \frac{\sum_{j=0}^{j=n} (O_j^T - O^T_{avg})(O_j^R - O^R_{avg})}{\sqrt{\sum_{j=0}^{j=n} (O_j^T - O^T_{avg})^2 \sum_{j=0}^{j=n} (O_j^R - O^R_{avg})^2}} \quad (7)$$

Where the summation is over different pairs of satellite-ozonesonde matchup values.

## 2.4 Estimation of Columnar Ozone

The total column ozone (TCO) from ozonesonde is calculated by integrating the ozone mixing ratio from the surface to burst altitude and then adding residual ozone above burst altitude. Here the residual ozone is obtained from satellite-derived balloon-burst climatology (BBC) (McPeters et al., 1997). The discrete integration for calculation of total ozone column (DU) between defined boundaries is performed as follows:

$$\text{Total column ozone} = 10^7 \times \left(\frac{RT_o}{g_o P_o}\right) \times \sum_{j=1}^{j=n} 0.5 \times (VMR[i] + VMR[i + 1]) \times (P[i] - P[i + 1]) \quad (86)$$

Where P is ambient pressure in hPa, VMR volume mixing ratio of ozone in ppbv, R (= 287.3 JKg<sup>-1</sup>K<sup>-1</sup>) gas constant, g<sub>o</sub> (= 9.88 ms<sup>-2</sup>), P<sub>o</sub> (= 1.01325×10<sup>5</sup> Pa) and T<sub>o</sub> (= 273.1 K) standard temperature.



776 The UTLS ozone column (DU) is also calculated using Eq. (86), where the UTLS region is defined  
 777 between 400 hPa to 70 hPa (Bian et al., 2007). Additionally, the tropospheric ozone column (DU)  
 778 is calculated for ozonesonde utilizing ~~the~~ Eq. (86) with boundaries from the surface to the  
 779 tropopause. The tropopause height from balloon-borne observations is estimated using the lapse  
 780 rate method as well as the AIRS-derived tropopause is used and shown in Figure 3. However, for  
 781 OMI and MLS tropospheric ozone residual method is used, which calculates the tropospheric  
 782 ozone column by subtracting the OMI total column from MLS stratospheric ozone column  
 783 (Hudson et al., 1998; Ziemke et al., 2006).

784  
 785  
 786  
 787

### 788 3. Results and Discussion

#### 789 3.1 Ozone Distribution ~~along~~ Along Balloon Trajectory: Ozonesonde and AIRS

790 The distributions of ozone along the balloon tracks obtained using all ozone soundings data during  
 791 four seasons are shown in Figure 4. The nearest swath of AIRS ozone observations is interpolated  
 792 to the balloon locations and ~~altitude are also shown~~ altitudes. Altitude variations of the balloon  
 793 along longitude ~~is~~ are shown in Figure S3. The balloons drift to a very long ~~distance~~  
 794 winter, followed by autumn and spring. During these seasons, ~~often~~ balloons often reach Nepal  
 795 also. The wind reversal ~~takes~~ took place during the summer-monsoon when the balloon ~~drifted~~  
 796 drifts towards IGP regions (Figure 4). The distributions of ozone from AIRS are more ~~or less~~  
 797 similar to the distributions those from ozonesonde. ~~This~~ Here, the ozone ~~variation reflects is~~  
 798 ~~tem~~ variations are reflecting in terms of spatial as well as vertical distributions. The bias and

822 coefficient of determination ( $r^2$ ) between ozonesonde and AIRS ozone ~~is~~are studied along the  
 823 longitude and latitude (Figures S3 and S4). Lower biases (lesser than 10%) and higher  $r^2$  are seen  
 824 in the lower and middle troposphere. The poor correlation ( $<0.4$ ) and larger biases of up to 28%  
 825 are seen at certain longitudes ~~those~~that are associated with higher altitudes ( $> 20$  km). Around the  
 826 balloon launch site (Nainital, 79.45 E) highest  $r^2$  score of 0.98 and low bias of 1.4% ~~is~~are observed,  
 827 which remain higher ( $r^2$ ) and lower (bias) up to 80° E (Figure S3).

828

829

830

### 831 3.2 Ozone Soundings and AIRS Ozone Profiles

832 Figure 5 shows the average monthly ozone profiles for collocated observations of ozonesonde and  
 833 AIRS, respectively, during seven-year periods. The ozonesonde convolved with AIRS averaging  
 834 kernels [ozonesonde (AK)] and AIRS a--priori are also compared. The value of percentage  
 835 difference between ozonesonde and AIRS ozone at 706, 617, 496, 103, 29, and 14 hPa altitudes  
 836 are shown in ~~the~~figure 5, and the zoomed variations in the lower tropospheric ozone (surface to  
 837 200 hPa) are also presented in the insets. AIRS slightly ( $\sim 10\%$ ) ~~underestimate~~underestimates  
 838 ozone in the lower troposphere during most of the months, except the summer-monsoon (June-  
 839 August), where an overestimation of up to 20% is observed. In the middle troposphere, around 300  
 840 hPa, an underestimation in the range ~~of~~ 1 - 17% is seen for all months with an approaching  
 841 tendency of ozonesonde (AK) towards the true ozonesonde profiles. However, near the tropopause  
 842 region, AIRS retrievals considerably overestimate ozone by up to 102%. The overestimation was  
 843 ~~the~~ highest for the winter season (82 - 102%), followed by the spring, ~~and~~ autumn, ~~and the~~  
 844 ~~while~~ lowest for the summer-monsoon season (10 - 27%). In the stratosphere, where the sensitivity

868 of AIRS is higher (Figure 2c), the ozonesonde and AIRS differences were relatively ~~lower~~  
869 ~~with lesser. Additionally, AIRS retrieval shows~~ an underestimation ~~in-between of~~ 5 - 21% ~~in this~~  
870 ~~altitude region.~~

871

872 As expected, the difference between ozonesonde and AIRS is significantly reduced (Table 1) after  
873 applying the averaging kernel or accounting for the sensitivity difference. This reduction was more  
874 notable for the summer monsoon period near the tropopause, where the difference reduced from  
875 92% to 19%, providing ~~an~~ improvement ~~by of~~ 72%. The improvement is as high as 100% on ~~a~~

876 monthly basis. Additionally, relative difference profiles were also analyzed for individual  
877 soundings as well for the different seasons (Figure S5). Higher differences of about 150% between  
878 AIRS and ozonesonde ozone observations were seen in the upper troposphere and lower  
879 stratospheric (UTLS) region. The higher difference during winter and spring between these  
880 observations in the UTLS region could be due to recurring ozone transport via tropopause folding  
881 over the observation site. Such events may remain undetected by AIRS due to lower vertical  
882 resolution leading to ~~the~~ missing of some tropopause folding events at lower altitudes (Figure 3).

883 However, in the lower troposphere, larger differences between ozonesonde and AIRS during  
884 summer-monsoon are seen, which are due to low ozone and frequent cloudy conditions leading to  
885 poor retrieval. The arrival of cleaner oceanic air during ~~the~~ south-west monsoon (or summer  
886 monsoon) brings ozone ~~-poor~~ air and frequent cloudy conditions over ~~the~~ northern India that  
887 weakens the photochemical ozone production (Naja et al., 2014; Sarangi et al., 2014). Moreover,

888 in the lower troposphere, the limited sensitivity of hyperspectral satellite instruments has ~~a~~  
889 significant contribution from the a ~~-~~priori information, which is also observed for AIRS retrieval  
890 (Figure 5).

914

915 Figure 6 shows the yearly time series analysis of the average ozone mixing ratio at four defined  
916 layers, characterizing the middle troposphere (600 - 300 hPa), the upper troposphere (300 - 100  
917 hPa), lower stratosphere (100 - 50 hPa), and middle stratosphere (50 - 10 hPa) respectively. A  
918 prominent seasonality was seen in the time series throughout the years, which is quite clear in the  
919 upper troposphere (300 - 100 hPa). The ozone seasonality contrast reflects the influence of  
920 summer-monsoon and winter seasons. The seasonality contrast is similar between AIRS and  
921 ozonesonde measurements, while a reversal of ozone seasonality is observed in the middle  
922 stratospheric region compared to other layers. The opposite seasonality of the middle stratospheric  
923 region is primarily due to dominant circulations, variation of solar radiation and dynamics. Total  
924 column water vapor ~~and monsoon index~~ is also shown in Figure 6 ~~and both show that shows~~ a  
925 tendency of anti-correlation with ozone in the 300 - 100 hPa region. ~~The monsoon index is~~  
926  
927 We have also estimated ~~(Wang et al., 2001)~~the monsoon index by the difference between zonal  
928 (U) wind (MERRA-2) at 850 hPa over the Arabian Sea (40 E – 80 E, 5 N – 15 N) and over the  
929 central Indian landmass (70 E - 90 E, 20 N – 30 N) as done by Wang et al. (2001).  
930 ~~). The anti-correlation with total column water vapor is slightly higher for AIRS ozone (-0.26) and~~  
931 ~~it is somewhat lower with ozonesonde (-0.15) in 300-100 hPa region. The relative difference of~~  
932 ~~AIRS ozone with ozonesonde in the upper tropospheric region also shows an anti-correlation~~  
933 ~~(Figure S6) of 0.17 with total column water vapor and of 0.27 with monsoon index, respectively.~~  
934  
935 In general, the positive values of the monsoon index correspond to strong ~~monsoon,~~monsoons and  
936 negative values correspond to weak monsoon periods (Wang et al., 2001). During the weak

959 monsoon, there is relatively drier air, lower cloud cover and higher surface temperature compared  
960 to the strong monsoon period (Lu et al., 2018). We observed ~~an anti-correlation (-0.49) between~~  
961 ~~yearly a tendency of lower annual~~ average ozone ~~(from ozonesonde and AIRS measurements)~~  
962 ~~during greater (positive) monsoon index- and higher annual average ozone during lower (negative)~~  
963 ~~monsoon index. Lu et al. (2018) have shown an anti-correlation (0.46) of tropospheric ozone with~~  
964 ~~monsoon index over the Indian region. The years 2011, 2012, 2014, and 2015 are classified as~~  
965 ~~weak monsoon years and relatively higher ozone is seen during these years, whereas for the years~~  
966 ~~2013, 2016, and 2017, strong monsoon is observed, and average yearly ozone was lesser during~~  
967 ~~these years (Figure 6 bottom left). The relative difference of AIRS ozone with ozonesonde in the~~  
968 ~~upper tropospheric region also shows an anti-correlation (Figure 6) of 0.17 with total column water~~  
969 ~~vapor.~~ Furthermore, the larger ozone differences between AIRS and ozonesonde ~~is~~are associated  
970 with the lower water vapor, ~~(Figure S6),~~ which may be arising due to the influence of ozone-  
971 sensitive water vapor (WV) channels in mid-Infra-red regions. Further, in the middle troposphere  
972 (600-300 hPa), a secondary ozone peak in post-monsoon is observed, which is suggested to be  
973 influenced by the ~~-~~biomass burning (Figure S7) over northern India that seems to be missing in the  
974 AIRS ozone.

975  
976 In the middle troposphere (600 - 300 hPa) and lower stratosphere (-100 - 50 hPa), AIRS retrievals  
977 show higher differences with respect to ozonesondes, while a nominal difference is observed for  
978 ~~the~~ middle troposphere and middle stratosphere- (Figure S6). Furthermore, a systematic increase  
979 ~~of in~~ standard deviation is also seen with the altitude. The higher standard deviations in the  
980 upper tropospheric and stratospheric regions are mainly due to higher ozone variability associated

1004 with stratosphere-troposphere exchange (STE) processes over the Himalayan region (Naja et al.,  
1005 2016; Bhardwaj et al., 2018).

1006

### 1007 3.3 Statistical Analysis of AIRS Ozone Profiles

1008 Error analysis of AIRS retrieved ozone over the Himalayan region is performed with spatio-  
1009 temporal collocated ozonesonde observations as a reference. The methodology to calculate the  
1010 root mean square error (RMSE), bias, and standard deviation (STD) is described in section 2.3.

1011  $W_2$  weighting statistics ~~is~~are utilized due to abrupt changes ~~of~~in atmospheric ozone with altitude.

1012 Here bias and STD between AIRS and ozonesonde are calculated at different RTA layers from  
1013 surface to 10 hPa. Figure 7 shows the average variation of bias and STD at different RTA layers

1014 from surface to 10 hPa over this region. The mean biases between ozonesonde and MLS, a high

1015 vertical resolution satellite instrument, ~~is~~are also shown in figure 7. In general, higher positive

1016 biases ( $\sim 65\%$ ) and STDs ( $\sim 25\%$ ) in AIRS ozone ~~is~~ retrieval are seen in the UTLS region, where

1017 MLS agrees well with ozonesonde. In the lower and middle troposphere, the AIRS ozone retrieval

1018 is negatively biased (0 - 25%), which increases gradually from the surface to higher altitudes ( $\sim$

1019 350hPa). A negative bias was also seen in the stratosphere of about 15%. Similar to the biases,

1020 STDs are also smaller in the lower troposphere and stratosphere, with values of nearly 15%. The

1021 higher statistical errors in the upper troposphere and the lower stratospheric region could be due

1022 to lower ozone partial pressure and frequent stratospheric to tropospheric transport events over the

1023 Himalayas (Rawat et al., 2020, 2021), which introduces ~~error~~ errors either after a mismatch of

1024 events in AIRS coarser vertical resolution or due to complex topography. Additionally, the AIRS

1025 tropopause frequency distribution shows less ability of AIRS to capture deep intrusion events

1026 (Figure 3). Further, AIRS trace gas retrieval largely depends on successful temperature retrieval

1050 and uses temperature retrieval as an input parameter (Maddy and Barnett, 2008). Hence,  
1051 temperature retrieval error could also propagate to ozone, and statistical error analysis of AIRS  
1052 temperature shows relatively higher biases ( $\sim 2$  K) in the upper tropospheric region (Figure S8).

1053

1054 The statistical error analysis was more-or-less similar for both true and smoothed ozonesonde  
1055 profiles. However, notable reduction in tropospheric bias and vertical shifts of errors were also  
1056 observed after applying the averaging kernel matrix to the true ozonesonde throughout the profile.  
1057 A shift of the error peak is seen from the lower stratosphere to the upper troposphere. This could  
1058 be due to the higher sensitivity of AIRS retrieval in the lower stratosphere, which would have  
1059 minimized the error at these particular altitudes. However, in the upper troposphere, higher  
1060 contribution of a-priories, as well as other factors (i.e., STE,) might have resulted in larger biases  
1061 and errors.

1062

1063 The histogram of differences between AIRS and ozonesonde (AK) is also studied at various  
1064 defined layers (Figure 8). AIRS mostly ~~underestimates~~underestimated ozone with a mean bias of  
1065 2.37 ppbv, 9.29 ppbv, and 39.8 ppbv in 800 - 600 hPa, 600 - 300 hPa, and 100 - 50 hPa layers,  
1066 respectively, while in the upper troposphere (300 - 100 hPa) AIRS overestimated with a mean bias  
1067 of 43.22 ppbv. Furthermore, distributions of differences are skewed ~~towards~~toward the negative  
1068 values in the lower stratosphere and towards positive values in the upper troposphere. ~~More~~A more  
1069 symmetric distribution over the negative axis is observed in the middle and lower troposphere. We  
1070 also studied the correlation profiles for different seasons (Figure 8, right panel). A strong  
1071 correlation is seen in the lower and middle troposphere for spring and summer, while there is a  
1072 poor correlation for winter and autumn. In the lower troposphere, a larger difference between AIRS

1096 and ozonesonde(AK) is observed, particularly during summer, with a relatively higher correlation  
1097 mostly due to the greater concurrence of AIRS a-priori with ozonesonde(AK). Whereas, in the  
1098 upper troposphere (300 - 100 hPa), a larger difference during winter and spring is primarily due to  
1099 frequent subtropical dynamics, while a higher correlation during the winter is mainly contributed  
1100 from the AIRS retrieval. Furthermore, analysis of the correlation coefficient between AIRS and  
1101 ozonesonde over different regions shows a higher value-correlation in the middle stratosphere  
1102 (0.95) and lower stratosphere (0.92), followed by in the upper troposphere (0.68), the lower  
1103 troposphere (0.62), and middle troposphere (0.47).

1104

### 1105 3.4 Assessment of AIRS Retrieval Algorithm with IASI and CrIS Radiance

1106 The MetOp/IASI and Soumi-NPP/CrIS radiance-based ozone products are assessed using  
1107 ozonesonde data over the central Himalayan region for one year (April 2014 to April 2015),  
1108 utilizing a total of 32 soundings. Here, the IASI and CrIS based ozone retrievals are research  
1109 products provided by NOAA, whose retrieval is based on the AIRS retrieval algorithm and follows  
1110 a similar averaging kernels matrix (Nalli et al., 2017). For IASI, due to the 09:30 ascending nodes  
1111 (morning overpass in India),  $\pm 6$  h loose temporal collocation is used. However, CrIS and AIRS  
1112 follow the same collocation due to a similar noontime overpass. The IASI, CrIS, and AIRS sensors  
1113 have 8461, 1305, and 2378 IR channels, respectively. Hence, analyzing their satellite ozone  
1114 products further helps to assess the AIRS retrieval algorithm for different IR radiances and channel  
1115 sets.

1116

1117 Figure 9a shows the seasonal ozone profiles obtained from three IR satellite sensors along with  
1118 ozonesonde for one year period. All sensors showed more-or-less similar ozone peak altitude and



1142 ozone gradient. The estimated ozone peak altitude for ozonesonde, AIRS, IASI, and CrIS are 11.35  
1143 hPa, 10 hPa, 9.11 hPa, and 7.78 hPa, respectively. The estimated ~~annual~~ average ozone gradient  
1144 in regions between tropopause to gradient peak are 231.5 ppbv/hPa, 199.0 ppbv/hPa, 193.2  
1145 ppbv/hPa, and 199.1 ppbv/hPa for ozonesonde, AIRS, CrIS, and IASI, respectively.

1146  
1147 ~~Higher~~ Moreover, the higher ozone ~~concentrations~~ values during spring throughout the troposphere  
1148 are captured well by all satellite sensors. Higher ozone during spring and winter in the UTLS  
1149 region ~~are is~~ observed well by AIRS and IASI, similar to ozonesonde but ~~not by such features seem~~  
1150 to be missing in CrIS ozone retrieval. At the same time, CrIS sensitivity looks relatively low, where  
1151 the possible role of the number of channels can be seen. However, IASI and AIRS have effectively  
1152 captured the ozone seasonal variability.

1153  
1154 Figure 9b shows the weighted statistical error analysis of IASI, CrIS, and AIRS ozone retrieval  
1155 with the true ozonesonde observations. Here, the difference in sensitivity of the two data sets is  
1156 not accounted for as this section's primary aim is to assess the AIRS retrieved algorithm using  
1157 different IR sensor radiances and channel sets. All three space-borne sensors overestimated UTLS  
1158 ozone by more than 50%, however, in the stratosphere and lower troposphere, the bias was slightly  
1159 lower, and it is somewhat underestimated. Similar to bias, the ~~STD~~ STDs were also higher in the  
1160 UTLS region by more than 60%. A consistent larger ~~error~~ differences in the UTLS region for all  
1161 three IR satellite sensors that share the ~~same~~ similar radiative transfer model and retrieval  
1162 algorithm shows the possible influence of complex topography and the various STE processes, in  
1163 introducing errors in retrieval processes, apart from input a-priories of the retrieval.

1164

1188 Additionally, Pearson correlations between ozonesonde and IASI, CrIS, and AIRS are also studied  
1189 at five atmospheric layers (i.e., 600-800 hPa, 300-600 hPa, 100-300 hPa, 50-100 hPa, and 10 - 50  
1190 hPa) (Table 2). A relatively stronger positive correlation is found in the middle stratosphere (50-  
1191 100 hPa) and lower stratosphere (50 - 100 hPa), which was highest for AIRS, followed by CrIS  
1192 and IASI, and a relatively low correlation is observed in the middle troposphere (300-600 hPa) for  
1193 AIRS and IASI (~ 44% and 31%), while CrIS shows the poorest correlation in the lower  
1194 troposphere about 9%. The lower concurrence between ozonesonde and the satellite sensors in the  
1195 lower troposphere could be due to lower sensitivity and shorter ~~life-time~~lifetime of near-surface  
1196 ozone that could increase the a-priori contribution and sampling mismatch, respectively.

1197

### 1198 3.5 Columnar Ozone

#### 1199 3.5.1 Total Column Ozone (TCO)

1200 Figure 10a shows variations in monthly average total column ozone (TCO) from ozonesonde,  
1201 AIRS, and OMI during 2011 - 2017. Here the box plots are also overlaid on the mean column to  
1202 describe the distribution of monthly column data. In general, the TCO is higher during spring,  
1203 which subsequently drops in summer-monsoon. AIRS TCO shows a bimodal monthly variation  
1204 which is not seen in the ozonesonde and OMI observations, otherwise, its monthly variation is in  
1205 reasonable agreement with ozonesonde. The OMI TCO ~~are-is~~ is in a good match with the ozonesonde  
1206 with a maximum difference of up to about 5 DU. Table 3 shows the difference in the TCO between  
1207 AIRS, OMI, and ozonesonde. AIRS shows considerable overestimation in the range of 2.2 - 22  
1208 DU for some months while notable underestimation (1.8 - 4 DU) for others, with respect to both  
1209 ozonesonde and OMI. The correlation between AIRS TCO and ozonesonde TCO is found to be  
1210 0.5 (Table S4). To further understand the cause of bimodal variations in AIRS (higher ozone during

1234 August, September, and October), the AIRS ozone profiles were integrated between different  
1235 stratospheric ~~region~~regions (100 -- 70 hPa, 70 - 50 hPa, 50 - 20 hPa, and 20 -- 1 hPa) and we  
1236 found that the elevated total ozone during post-monsoon is mainly contributed from the altitude  
1237 above 50 hPa.

1238

### 1239 3.5.2 UTLS Ozone Column

1240 Figure 10b shows the variations in the monthly average UTLS ozone column for collocated and  
1241 concurrent observations of AIRS, MLS, and ozonesonde during 2011 - 2017. The UTLS region  
1242 extends between 400 hPa to 70 hPa (Bian et al., 2007) for ozonesonde and AIRS, while for MLS  
1243 , the region between 261 hPa to 70 hPa is utilized. The recommended pressure levels for MLS v4  
1244 ozone retrieval ~~is~~are above 261 hPa (Livesey et al., 2013; Schwartz et al., 2015). In contrast to  
1245 TCO, ~~a~~ higher ozone in UTLS is seen during the winter and spring (~ 45 DU) when there are  
1246 recurring downward transport events, while a clear drop of the column during the summer-  
1247 monsoon shows the convective transport of cleaner oceanic air to the higher altitudes. All the  
1248 collocated observations are able to capture the monthly variation effectively; ~~however.~~ However,  
1249 there is a substantial overestimation by more than 3 DU (Table S5) for all the months in ~~-~~AIRS  
1250 measurements; ~~while~~ and MLS mostly underestimate it, except during winter due to smaller  
1251 integrated columns. Further more, the larger whiskers of the box plot during winter and spring show  
1252 the larger variations of the ozone in the UTLS region. Though there were notable overestimations  
1253 compared to ozonesonde, still UTLS monthly variations are captured well by AIRS with a  
1254 correlation of up to 75% (Table S4). In addition, the correlation of ozonesonde and AIRS ozone at  
1255 each pressure ~~levels~~level in the UTLS region is 0.81, which further increases with  
1256 ozonesonde(AK) (of about 0.94). The persistent biases in the satellite retrievals arises due to

1280 inadequate input parameters that can be improved by using more accurate initial parameters and  
1281 surface emissivity (Dufour et al., 2012; Boynard et al., 2018).

1282

1283

### 1284 3.5.3 Tropospheric Ozone Column

1285 Figure 10c shows the variations in the monthly average tropospheric ozone column utilizing  
1286 various collocated data sets during 2011 - 2017. The tropospheric ozone column is calculated by  
1287 integrating ozone profiles from the surface to the tropopause. WMO-defined lapse rate calculation  
1288 method is used to calculate tropopause height from balloon-borne and AIRS observations (Figure  
1289 3). Higher tropospheric ozone is observed during the spring and early summer (> 45 DU) when  
1290 annual crop-residue burning (Figure S7) events occur over northern India, apart from downward  
1291 transport from the stratosphere. ~~Few~~A few cases of downward transport are discussed in the next  
1292 section. The tropospheric ozone column drops rapidly during the summer-monsoon when pristine  
1293 marine air reaches Nainital. A slight increase of column is also seen during the autumn, which is  
1294 again influenced by post-monsoon crop residue burning practices (Figure S7) ~~in~~over northern India  
1295 (Bhardwaj et al., 2016). The AIRS is able to capture the monthly variations very effectively;  
1296 however, there are larger biases. The biases with ozonesonde are higher when the tropopause is  
1297 taken from the balloon-borne observation, while with AIRS provided tropopause, the biases are  
1298 lesser or mostly within the one sigma limit. The correlation between ozonesonde and AIRS, when  
1299 used AIRS tropopause, is very strong (0.72). Like AIRS, the OMI/MLS column is in good  
1300 agreement and able to produce monthly variations; however, there are larger differences during  
1301 winter and spring of more than 10 DU. The tropospheric ozone column from ozonesonde is  
1302 different for balloon-borne LRT and AIRS tropopause, ~~whose possible reason~~which could be due

1326 to the lower vertical resolution of AIRS, ~~which~~. AIRS calculates tropopause with an uncertainty  
1327 of 1-2 km (Divakarla et al., 2006), ~~and~~. It can also be seen that on average a lower (about 28%)  
1328 tropopause pressure (or higher altitude) ~~by 28%~~ is calculated by AIRS compare to ozonesonde  
1329 measurements (Figure 3).

1330

### 1331 3.6 Case Studies of Biomass Burning and Downward Transport

1332 Over ~~the~~ northern India, extensive agriculture practices and forest fires influence ozone at the  
1333 surface and higher altitudes (Kumar et al., 2011; Cristofanelli et al., 2014; Bhardwaj et al., 2016;  
1334 Bhardwaj et al., 2018). Based on MODIS fire counts, the days in between 1 March to 15 April  
1335 over northern India are classified as the low fire periods (LFP) as considered in previous studies  
1336 over this region. The high fire period (HFP) is classified when the fire counts over the  
1337 observational site are more than the median fire counts in the biomass burning period, typically  
1338 from mid-April to May (Bhardwaj et al., 2016). A total of 32 soundings (mid-April to May) are  
1339 classified as HFP and 33 soundings (March to mid-April) are classified as LFP. Figure 11 (left)  
1340 shows the average ozone profiles up to 6 km from ozonesonde and AIRS observations during HFP  
1341 and LFP. The ozonesonde data show enhancement in ozone by about 5 ppbv to about 11 ppbv  
1342 during HFP as compared to LFP that is accounting ~~to~~ for a 5-20% increase. It is important to  
1343 mention that enhancement is greater at higher altitude ~~region~~. regions that drop gradually above  
1344 400 hPa. The enhancement is slightly lower (10-15%) in the AIRS profile, where most of it is  
1345 contributed by the a-priori profile (Figure S8).

1346

1347 Deep stratospheric intrusion or the downward transport (DT) of ozone-rich air from the  
1348 stratosphere to the troposphere significantly influences ozone profiles over the subtropical regions

1372 (Collins, et al., 2003; Zhu, et al., 2006; Lal et al., 2014). Over the subtropical Himalayas, such  
1373 ozone intrusions are observed during the winter and ~~the~~ spring seasons (Zhu et al., 2006; Ojha et  
1374 al., 2014). The DT events are classified based on the higher ozone in middle - upper troposphere  
1375 seen from ozonesonde with relatively larger Ertel potential vorticity (EPV) and lower humidity in  
1376 MERRA-2 reanalysis data. Based on this, 10 soundings (between January and mid-April) are  
1377 classified as DT events for ozonesonde and AIRS. Figure 11 (right) shows ozone profiles from  
1378 ozonesonde (AK) and AIRS observations for high ozone DT events as well as the average ozone  
1379 profiles of corresponding months excluding the DT event. Though there are persistent positive  
1380 biases in AIRS ozone profile compared to ozonesonde in the middle/upper troposphere, still both  
1381 the observations have captured the influence of the downward transport on the ozone profile very  
1382 effectively and show an increase in the ozone of 10 - 20% in altitude range 2 - 16 km. Ozonesonde  
1383 based observations have shown about ~~two-fold~~twofold increase in upper-middle tropospheric  
1384 ozone due to downward ozone transport over this region (Ojha et al., 2014). Further, the first guess  
1385 profile's contribution to AIRS retrieval during DTs is negligible (Figure S9) and shows the main  
1386 contribution from the AIRS observations itself. So, despite the persistent biases in the AIRS and  
1387 ozonesonde observations, AIRS is able to capture the influences of downward transport (DT) on  
1388 ozone profile notably well.

1389

### 1390 **3.7 Ozone Radiative Forcing**

1391 Radiative forcing is a valuable metric to estimate the radiative impacts of any anthropogenic or  
1392 natural activity on the climate system (Ramaswamy et al., 2001). It measures the net radiation at  
1393 the surface, tropopause, and the top of the atmosphere due to any atmospheric constituents. Here  
1394 we discuss the ozone radiative forcing (RF) at the surface in the ultraviolet (UV) spectral range

1418 (Antón et al., 2014; Mateos et al., 2020) using the ozonesonde, OMI, and AIRS total column ozone  
1419 (TCO) data. The RF is calculated based on Antón et al. (2014), relative to 1979 utilizing TOMS  
1420 TOC data in 1979, monthly averaged solar zenith angles of site, clearness index based on  
1421 Chakraborty et al., (2014) and Hawas et al., (1984), and respective monthly average TCO data of  
1422 AIRS, OMI, and ozonesonde. Rather than quantifying the RF values here, our primary focus is to  
1423 show how the discrepancies of satellite ozone data (mainly AIRS) can impact the calculation of  
1424 RF values. Figure 12 shows the seasonal average ozone radiative forcing (RF) relative to 1979.  
1425 The annual average ozone RF during 2011 -2017 is 4.86, 4.04, and 2.96 mW/m<sup>2</sup> for ozonesonde,  
1426 OMI, and AIRS, respectively. The RF values for ozonesonde and OMI are comparable to Mateos  
1427 et al. (2020) (4 mW/m<sup>2</sup>) for the extratropical region. However, for AIRS, the RF value is lower by  
1428 45%. Further, the seasonal average ozone RF (2011-2017) is consistent between ozonesonde and  
1429 OMI, while notable differences are seen in AIRS except during the winter season when differences  
1430 are marginal (Figure 12). Also from Table 3, it is clear that the higher total ozone bias during  
1431 autumn (as high as 22 DU) contributes to higher RF differences in autumn (Figure 12).

1432

#### 1433 **4. Summary and Conclusions**

1434 This study has utilized 242 ozone soundings (during 2011 - 2017) conducted over the Himalayan  
1435 station (Nainital) to evaluate the AIRS version 6 ozone product and study the performance during  
1436 biomass burning events, ozone downward transport events and estimation of ozone radiative  
1437 forcing. AIRS ozone retrieval is evaluated in terms of retrieval sensitivity, retrieval biases, retrieval  
1438 errors, and ability to retrieve the natural variability of columnar ozone at different altitude regions.  
1439 This study is the first of its kind in the Himalayan region. The AIRS averaging kernels information  
1440 was applied to ozonesonde for a like-for-like comparison to overcome their sensitivity differences.

1464 The monthly profile evaluation shows ozone peak and ozone altitude dependency is captured well  
1465 by AIRS retrieval with smaller but notable underestimation (5 - 20%) in the lower-middle  
1466 troposphere and stratosphere, while overestimation in the UTLS region as high as 102%. We show  
1467 the larger sensitivity of AIRS ozone for the summer monsoon in the UTLS region, where the biases  
1468 between AIRS and ozonesonde improved remarkably after applying AIRS averaging kernel  
1469 information.

1470  
1471 The weighted statistical error analysis of AIRS retrieved ozone profiles shows higher positive  
1472 biases (65%) and STD (25%) in the upper troposphere. In the lower and middle troposphere, AIRS  
1473 ozone was negatively biased, apart from the stratosphere. In addition, though the biases and errors  
1474 are higher in the upper troposphere, there is a larger correlation of about 81% showing the  
1475 capability of AIRS to retrieve upper tropospheric ozone variability with certain positive biases that  
1476 can be eliminated by choosing better emissivity inputs or other retrieval inputs. The AIRS ozone  
1477 retrieval algorithm was further evaluated using the radiance of IASI and CrIS sensors; these  
1478 sensors provided similar error statistics as seen for AIRS.

1479  
1480 The AIRS-derived columnar ozone amounts (i.e., total, UTLS, and tropospheric ozone) are also  
1481 evaluated to see whether the ozone variability at different altitude regions is being retrieved  
1482 correctly. The UTLS and tropospheric ozone monthly variations are captured well by AIRS with  
1483 ~~persistence~~persistent positive biases. However, the total ozone column shows bimodal monthly  
1484 variations, which was not evident in the ozonesonde and OMI total ozone observations. Further,  
1485 we found a higher total ozone column in AIRS during autumn, which is mostly coming from the  
1486 stratospheric region above 50 hPa. The capabilities of AIRS to capture various biomass burning



1510 and downward transport events have also been studied. AIRS captures all such events reasonably  
1511 well with notable contributions of the a-priori, particularly in the biomass burning events.

1512  
1513 Unlike the well-mixed greenhouse gases, the ozone radiative forcing (RF) remains uncertain due  
1514 to inadequate budget estimates and complex chemical processes. The total ozone discrepancies of  
1515 AIRS lead to show lower RF (by about 45%) and greater uncertainty in this Himalayan region.  
1516 Stevenson et al. (2013) have shown that a few percent uncertainties in ozone concentrations can  
1517 produce a spread of ~17% in ozone RF estimations. Here, the role of in-situ observations from  
1518 ozone soundings is shown to be important in improving the satellite retrieved ozone over the  
1519 Himalayan region by assessing and providing insights upon its error and bias. This information  
1520 could be applied ~~for~~to the ozone ~~product~~retrieval from other satellite data ~~set,sets~~, having long-  
1521 term coverage. This will help in better understanding regional ozone and radiation budgets over  
1522 this Himalayan region having complex topography.

1523

#### 1524 **Acknowledgments**

1525 ~~This work is supported by the~~We are grateful to Director ARIES and ISRO-ATCTM project for  
1526 supporting this work. Help from Deepak and Nitin in balloon launches and coordination with the  
1527 air traffic control is highly acknowledged. ~~We are grateful to Director ARIES for supporting this~~  
1528 ~~work.~~The National Center for Atmospheric Research is sponsored by the National Science  
1529 Foundation. SL is grateful to INSA, New Delhi for the position and Director PRL, Ahmedabad for  
1530 the support. We highly acknowledge NOAA and NASA-EARTHDATA online data portals for  
1531 providing IASI, AIRS, and CrIS label2 data. We thank the NASA Goddard Space Flight Center  
1532 Ozone Processing Team for providing the OMI/MLS tropospheric ozone, OMI total ozone column

1557 and JPL for MLS ozone profile. We would also like to acknowledge the use of the MODIS fire  
1558 data through FIRMS archive download. Use of map from Google earth is also acknowledged. We  
1559 thank the reviewers for their constructive comments and valuable suggestions.

1560

1561

1562 **Data availability:** Satellite data are available in the respective web portal. Ozonesonde data could  
1563 be made available on a reasonable request by writing to the corresponding author.

1564

## 1565 **References**

1566 Antón, M., D. Mateos, R. Román, A. Valenzuela, L. Alados-Arboledas, and F. J. Olmo.: A method  
1567 to determine the ozone radiative forcing in the ultra-violet range from experimental data, J.  
1568 Geophys. Res. Atmos., 119, 1860–1873, doi:10.1002/2013JD020444, 2014.

1569

1570 Aghedo, A.M., Bowman, K.W., Worden, H.M., Kulawik, S.S., Shindell, D.T., Lamarque, J.F.,  
1571 Faluvegi, G., Parrington, M., Jones, D.B.A. and Rast, S.: The vertical distribution of ozone  
1572 instantaneous radiative forcing from satellite and chemistry climate models. Journal of  
1573 Geophysical Research: Atmospheres, 116(D1), 2011.

1574

1575 Bai, W., Wu, C., Li, J. and Wang, W.: Impact of terrain altitude and cloud height on ozone remote  
1576 sensing from satellite, Journal of Atmospheric and Oceanic Technology, 31(4), pp.903-912, 2014.

1577

1578 Barre, J., Peuch, V.H., Attié, J.L., Amraoui, L.E., Lahoz, W.A., Josse, B., Claeysman, M. and  
1579 Nedelec, P.: Stratosphere-troposphere ozone exchange from high resolution MLS ozone analyses,  
1580 Atmos. Chem. Phys., 12(14), pp.6129-6144, 2012.

1604

1605 Bhardwaj, P., Naja, M., Kumar, R. and Chandola, H.C.: Seasonal, interannual, and long-term  
1606 variabilities in biomass burning activity over South Asia, *Environmental Science and Pollution*  
1607 *Research*, 23(5), pp.4397-4410, 2016.

1608

1609 Bhardwaj, P., Naja, M., Rupakheti, M., Lupascu, A., Mues, A., Panday, A. K., Kumar, R., Mahata,  
1610 K. S., Lal, S., Chandola, H. C., and Lawrence, M. G.: Variations in surface ozone and carbon  
1611 monoxide in the Kathmandu Valley and surrounding broader regions during SusKat-ABC field  
1612 campaign: role of local and regional sources, *Atmos. Chem. Phys.*, 18, 11949–11971,  
1613 <https://doi.org/10.5194/acp-18-11949-2018>, 2018.

1614

1615 Bhartia, P.K., McPeters, R.D., Mateer, C.L., Flynn, L.E. and Wellemeyer, C.: Algorithm for the  
1616 estimation of vertical ozone profiles from the backscattered ultraviolet technique, *J. Geophys. Res.*  
1617 *Atmos.*, 101(D13), pp.18793-18806, 1996.

1618

1619 Bian, J., Gettelman, A., Chen, H. and Pan, L.L.: Validation of satellite ozone profile retrievals  
1620 using Beijing ozonesonde data, *J. Geophys. Res. Atmos.*, 112(D6), 2007.

1621

1622 Boynard, A., Hurtmans, D., Koukouli, M.E., Goutail, F., Bureau, J., Safieddine, S., Lerot, C.,  
1623 Hadji-Lazaro, J., Wespes, C., Pommereau, J.P. and Pazmino, A.: Seven years of IASI ozone  
1624 retrievals from FORLI: validation with independent total column and vertical profile  
1625 measurements, *Atmos. Meas. Tech.*, 9(9), pp.4327-4353, 2016.

1626

1650 Boynard, A., Hurtmans, D., Garane, K., Goutail, F., Hadji-Lazaro, J., Koukouli, M. E., Wespes,  
1651 C., Vigouroux, C., Keppens, A., Pommereau, J.-P., Pazmino, A., Balis, D., Loyola, D., Valks, P.,  
1652 Sussmann, R., Smale, D., Coheur, P.-F., and Clerbaux, C.: Validation of the IASI  
1653 FORLI/EUMETSAT ozone products using satellite (GOME-2), ground-based (Brewer–Dobson,  
1654 SAOZ, FTIR) and ozonesonde measurements, *Atmos. Meas. Tech.*, 11, 5125–5152,  
1655 <https://doi.org/10.5194/amt-11-5125-2018>, 2018.

1656  
1657 Chakraborty, S., Sadhu, P.K. and Nitai, P.A.L.: New location selection criterions for solar PV  
1658 power plant. *International Journal of Renewable Energy Research*, 4(4), pp.1020-1030, 2014.

1659  
1660 Clerbaux, C., Hadji-Lazaro, J., Turquety, S., George, M., Coheur, P.F., Hurtmans, D., Wespes, C.,  
1661 Herbin, H., Blumstein, D., Tourniers, B. and Phulpin, T.: The IASI/MetOp1 Mission: First  
1662 observations and highlights of its potential contribution to GMES2, *Space Research Today*, 168,  
1663 pp.19-24, 2007.

1664  
1665 Coheur, P.F., Barret, B., Turquety, S., Hurtmans, D., Hadji-Lazaro, J. and Clerbaux, C.: Retrieval  
1666 and characterization of ozone vertical profiles from a thermal infrared nadir sounder, *J. Geophys.*  
1667 *Res. Atmos.*, 110(D24), 2005.

1668  
1669 Collins, W. J., R. G. Derwent, B. Garnier, C. E. Johnson, M. G. Sanderson, and D. S. Stevenson.:  
1670 Effect of stratosphere-troposphere exchange on the future tropospheric ozone trend, *J. Geophys.*  
1671 *Res.*, 108(D12), 8528, doi:10.1029/2002JD002617, 2003.

1672

1696 Cristofanelli, P., Putero, D., Adhikary, B., Landi, T.C., Marinoni, A., Duchi, R., Calzolari, F., Laj,  
1697 P., Stocchi, P., Verza, G. and Vuillermoz, E.: Transport of short-lived climate forcers/pollutants  
1698 (SLCF/P) to the Himalayas during the South Asian summer monsoon onset, *Environmental*  
1699 *Research Letters*, 9(8), p.084005, 2014.

1700

1701 Divakarla, M., Barnet, C., Goldberg, M., Maddy, E., Wolf, W., Flynn, L., Xiong, X., Wei, J., Zhou,  
1702 L. and Liu, X.: Validation of Atmospheric Infrared Sounder (AIRS) temperature, water vapor, and  
1703 ozone retrievals with matched radiosonde and ozonesonde measurements and forecasts, In  
1704 *Multispectral, Hyperspectral, and Ultraspectral Remote Sensing Technology, Techniques, and*  
1705 *Applications*, International Society for Optics and Photonics, Vol. 6405, p. 640503, 2006.

1706

1707 Divakarla, M., Barnet, C., Goldberg, M., Maddy, E., Irion, F., Newchurch, M., Liu, X., Wolf, W.,  
1708 Flynn, L., Labow, G. and Xiong, X.: Evaluation of Atmospheric Infrared Sounder ozone profiles  
1709 and total ozone retrievals with matched ozonesonde measurements, ECMWF ozone data, and  
1710 Ozone Monitoring Instrument retrievals, *J. Geophys. Res. Atmos.*, 113(D15), 2008.

1711

1712 Dufour, G., Eremenko, M., Griesfeller, A., Barret, B., LeFlochmoën, E., Clerbaux, C., Hadji-  
1713 Lazaro, J., Coheur, P.F. and Hurtmans, D.: Validation of three different scientific ozone products  
1714 retrieved from IASI spectra using ozonesondes, *Atmos. Meas. Tech.*, 5(3), pp.611-630, 2012.

1715

1716 Ebi, K.L. and McGregor, G., Climate change, tropospheric ozone and particulate matter, and health  
1717 impacts, *Environmental health perspectives*, 116(11), pp.1449-1455, 2008.

1718

1742 Fadnavis, S., Dhomse, S., Ghude, S., Iyer, U., Buchunde, P., Sonbawne, S. and Raj, P.E.: Ozone  
1743 trends in the vertical structure of Upper Troposphere and Lower stratosphere over the Indian  
1744 monsoon region, International Journal of Environmental Science and Technology, 11(2), pp.529-  
1745 542, 2014.

1746

1747 Finlayson-Pitts, B.J. and Pitts, J.N.: Tropospheric air pollution: ozone, airborne toxics, polycyclic  
1748 aromatic hydrocarbons, and particles, Science, 276(5315), pp.1045-1051, 1997.

1749

1750 Fishbein, E., Farmer, C.B., Granger, S.L., Gregorich, D.T., Gunson, M.R., Hannon, S.E.,  
1751 Hofstadter, M.D., Lee, S.Y., Leroy, S.S. and Strow, L.L.: Formulation and validation of simulated  
1752 data for the Atmospheric Infrared Sounder (AIRS), IEEE Transactions on Geoscience and Remote  
1753 Sensing, 41(2), pp.314-329, 2003.

1754

1755 Fishman, J., Ramanathan, V., Crutzen, P.J. and Liu, S.C.: Tropospheric ozone and climate, Nature,  
1756 282(5741), pp.818-820, 1979.

1757

1758 Fishman, J., Minnis, P. and Reichle Jr, H.G.: Use of satellite data to study tropospheric ozone in  
1759 the tropics, J. Geophys. Res. Atmos., 91(D13), pp.14451-14465, 1986.

1760

1761 Fishman, J. and Larsen, J.C.: Distribution of total ozone and stratospheric ozone in the tropics:  
1762 Implications for the distribution of tropospheric ozone, J. Geophys. Res. Atmos., 92(D6), pp.6627-  
1763 6634, 1987.

1764

1786 Foret, G., Eremenko, M., Cuesta, J., Sellitto, P., Barré, J., Gaubert, B., Coman, A., Dufour, G.,  
1787 Liu, X., Joly, M. and Doche, C.: Ozone pollution: What can we see from space? A case study, J.  
1788 Geophys. Res. Atmos., 119(13), pp.8476-8499, 2014.

1789  
1790 Forster, P.M., Bodeker, G., Schofield, R., Solomon, S. and Thompson, D.: Effects of ozone cooling  
1791 in the tropical lower stratosphere and upper troposphere, Geophysical Research Letters, 34(23),  
1792 2007.

1793  
1794 Fry, M.M., Naik, V., West, J.J., Schwarzkopf, M.D., Fiore, A.M., Collins, W.J., Dentener, F.J.,  
1795 Shindell, D.T., Atherton, C., Bergmann, D. and Duncan, B.N.: The influence of ozone precursor  
1796 emissions from four world regions on tropospheric composition and radiative climate forcing.  
1797 Journal of Geophysical Research: Atmospheres, 117(D7), 2012.

1798 ~~Finlayson-Pitts, B.J. and Pitts, J.N.: Tropospheric air pollution: ozone, airborne toxics, polycyclic~~  
1799 ~~aromatic hydrocarbons, and particles, Science, 276(5315), pp.1045-1051, 1997.~~

1800  
1801 ~~Fishman, J., Ramanathan, V., Crutzen, P.J. and Liu, S.C.: Tropospheric ozone and climate, Nature,~~  
1802 ~~282(5741), pp.818-820, 1979.~~

1803  
1804 ~~Fishman, J., Minnis, P. and Reichle Jr, H.G.: Use of satellite data to study tropospheric ozone in~~  
1805 ~~the tropics, J. Geophys. Res. Atmos., 91(D13), pp.14451-14465, 1986.~~

1806

1829 ~~Fishman, J. and Larsen, J.C.: Distribution of total ozone and stratospheric ozone in the tropics:~~  
 1830 ~~Implications for the distribution of tropospheric ozone, J. Geophys. Res. Atmos., 92(D6), pp.6627-~~  
 1831 ~~6634, 1987.~~

1832  
 1833 Gauss, M., Myhre, G., Pitari, G., Prather, M.J., Isaksen, I.S.A., Bernsten, T.K., Brasseur, G.P.,  
 1834 Dentener, F.J., Derwent, R.G., Hauglustaine, D.A. and Horowitz, L.W.: Radiative forcing in the  
 1835 21st century due to ozone changes in the troposphere and the lower stratosphere, J. Geophys. Res.  
 1836 Atmos., 108(D9), 2003.

1837  
 1838 Hauglustaine, D.A. and Brasseur, G.P.: Evolution of tropospheric ozone under anthropogenic  
 1839 activities and associated radiative forcing of climate, J. Geophys. Res. Atmos., 106(D23),  
 1840 pp.32337-32360, 2001.

1841  
 1842 Hawas, M.M. and Muneer, T.; Study of diffuse and global radiation characteristics in  
 1843 India. Energy Conversion and Management, 24(2), pp.143-149, 1984.

1844  
 1845 Hudson, R.D. and Thompson, A.M.: Tropical tropospheric ozone from total ozone mapping  
 1846 spectrometer by a modified residual method, J. Geophys. Res. Atmos., 103(D17), pp.22129-  
 1847 22145, 1998.

1848  
 1849 Hegglin, M. I., Fahey, D. W., McFarland, M., Montzka, S. A., and Nash, E. R.: Twenty questions  
 1850 and answers about the ozone layer: 2014 update, Scientific Assessment of Ozone Depletion: 2014,



1873 84 pp., World Meteorological Organization, Geneva, Switzerland, ISBN 978-9966-076-02-1,  
1874 2015.

1875

1876 Irion, F.W., Kahn, B.H., Schreier, M.M., Fetzer, E.J., Fishbein, E., Fu, D., Kalmus, P., Wilson,  
1877 R.C., Wong, S. and Yue, Q.: Single-footprint retrievals of temperature, water vapor and cloud  
1878 properties from AIRS. *Atmospheric Measurement Techniques*, 11(2), pp.971-995, 2018.

1879

1880 Kim, J.H. and Newchurch, M.J.: Climatology and trends of tropospheric ozone over the eastern  
1881 Pacific Ocean: The influences of biomass burning and tropospheric dynamics, *Geophysical*  
1882 *research letters*, 23(25), pp.3723-3726, 1996.

1883

1884 Komhyr, W.D., Barnes, R.A., Brothers, G.B., Lathrop, J.A. and Opperman, D.P.: Electrochemical  
1885 concentration cell ozonesonde performance evaluation during STOIC 1989, *J. Geophys. Res.*  
1886 *Atmos.*, 100(D5), pp.9231-9244, 1995.

1887

1888 Komhyr, W.D.: Nonreactive gas sampling pump. *Review of Scientific Instruments*, 38(7), pp.981-  
1889 983, 1967.

1890

1891 Kumar, R., Naja, M., Satheesh, S.K., Ojha, N., Joshi, H., Sarangi, T., Pant, P., Dumka, U.C.,  
1892 Hegde, P. and Venkataramani, S.: Influences of the springtime northern Indian biomass burning  
1893 over the central Himalayas. *Journal of Geophysical Research: Atmospheres*, 116(D19), 2011.

1894

- 1917 Kumar, R., Naja, M., Pfister, G.G., Barth, M.C. and Brasseur, G.P.: Simulations over South Asia  
1918 using the Weather Research and Forecasting model with Chemistry (WRF-Chem): set-up and  
1919 meteorological evaluation, *Geoscientific Model Development*, 5(2), pp.321-343, 2012a.  
1920
- 1921 Kumar, R., Naja, M., Pfister, G.G., Barth, M.C., Wiedinmyer, C. and Brasseur, G.P.: Simulations  
1922 over South Asia using the Weather Research and Forecasting model with Chemistry (WRF-  
1923 Chem): chemistry evaluation and initial results, *Geoscientific Model Development*, 5(3), pp.619-  
1924 648, 2012b.  
1925
- 1926 Lacis, A.A., Wuebbles, D.J. and Logan, J.A.: Radiative forcing of climate by changes in the  
1927 vertical distribution of ozone, *J. Geophys. Res. Atmos.*, 95(D7), pp.9971-9981, 1990.  
1928
- 1929 Lal S., S. Venkataramani, S. Srivastava, S. Gupta, M. Naja, T. Sarangi, X. Liu.: Transport effects  
1930 on the vertical distribution of tropospheric ozone over the tropical marine regions surrounding  
1931 India, *J. Geophys. Res.*, 118, 1513-1524, doi:10.1002/jgrd.50180, 2013.  
1932
- 1933 Lal S., S. Venkataramani, N. Chandra, O. R. Cooper, J. Brioude, and M. Naja, Transport effects  
1934 on the vertical distribution of tropospheric ozone over western India, *J. Geophys. Res. Atmos.*,  
1935 119, doi:10.1002/2014JD021854, 2014.  
1936
- 1937 Lal, S., Venkataramani, S., Naja, M., Kuniyal, J.C., Mandal, T.K., Bhuyan, P.K., Kumari, K.M.,  
1938 Tripathi, S.N., Sarkar, U., Das, T. and Swamy, Y.V.: Loss of crop yields in India due to surface

1961 ozone: An estimation based on a network of observations, *Environmental Science and Pollution*  
1962 *Research*, 24(26), pp.20972-20981, 2017.

1963

1964 Lawrence, M.G. and Lelieveld, J.: Atmospheric pollutant outflow from southern Asia: a review,  
1965 *Atmospheric Chemistry and Physics*, 10(22), pp.11017-11096, 2010.

1966

1967 Lelieveld, J., Haines, A. and Pozzer, A.: Age-dependent health risk from ambient air pollution: a  
1968 modelling and data analysis of childhood mortality in middle-income and low-income countries,  
1969 *The lancet Planetary health*, 2(7), pp.e292-e300, 2018.

1970

1971 Livesey, N.J., Logan, J.A., Santee, M.L., Waters, J.W., Doherty, R.M., Read, W.G., Froidevaux,  
1972 L. and Jiang, J.H.; Interrelated variations of O<sub>3</sub>, CO and deep convection in the  
1973 tropical/subtropical upper troposphere observed by the Aura Microwave Limb Sounder (MLS)  
1974 during 2004–2011. *Atmospheric Chemistry and Physics*, 13(2), pp.579-598, 2013.

1975

1976 Logan, J.A.: Tropospheric ozone: Seasonal behavior, trends, and anthropogenic influence, *J.*  
1977 *Geophys. Res. Atmos.*, 90(D6), pp.10463-10482, 1985.

1978

1979 Lu, X., Zhang, L., Liu, X., Gao, M., Zhao, Y. and Shao, J., 2018. Lower tropospheric ozone over  
1980 India and its linkage to the South Asian monsoon. *Atmospheric Chemistry and Physics*, 18(5),  
1981 pp.3101-3118.

1982

- 2006 Maddy, E.S. and Barnet, C.D.: Vertical resolution estimates in version 5 of AIRS operational  
2007 retrievals, IEEE Transactions on Geoscience and Remote Sensing, 46(8), pp.2375-2384, 2008.  
2008
- 2009 Mateos, D. and Antón, M.: Worldwide Evaluation of Ozone Radiative Forcing in the UV-B Range  
2010 between 1979 and 2014. Remote Sensing, 12(3), p.436, 2020.  
2011
- 2012 McPeters, R.D., Miles, T., Flynn, L.E., Wellemeyer, C.G. and Zawodny, J.M.: Comparison of  
2013 SBUV and SAGE II ozone profiles: Implications for ozone trends, J. Geophys. Res. Atmos.,  
2014 99(D10), pp.20513-20524, 1994.  
2015
- 2016 McPeters, R.D., Labow, G.J. and Johnson, B.J.: A satellite-derived ozone climatology for  
2017 balloonsonde estimation of total column ozone, J. Geophys. Res. Atmos., 102(D7), pp.8875-8885,  
2018 1997.  
2019
- 2020 McPeters, R.D., Labow, G.J. and Logan, J.A.: Ozone climatological profiles for satellite retrieval  
2021 algorithms, J. Geophys. Res. Atmos., 112(D5), 2007.  
2022
- 2023 Monahan, K.P., Pan, L.L., McDonald, A.J., Bodeker, G.E., Wei, J., George, S.E., Barnet, C.D. and  
2024 Maddy, E.: Validation of AIRS v4 ozone profiles in the UTLS using ozonesondes from Lauder,  
2025 NZ and Boulder, USA, J. Geophys. Res. Atmos., 112(D17), 2007.  
2026
- 2027 Monks, P.S., Archibald, A.T., Colette, A., Cooper, O., Coyle, M., Derwent, R., Fowler, D.,  
2028 Granier, C., Law, K.S., Mills, G.E. and Stevenson, D.S.: Tropospheric ozone and its precursors

2052 [from the urban to the global scale from air quality to short-lived climate forcer. Atmospheric](#)  
2053 [Chemistry and Physics, 15\(15\), pp.8889-8973, 2015.](#)

2054

2055 Munro, R., Siddans, R., Reburn, W.J. and Kerridge, B. J.: Direct measurement of tropospheric  
2056 ozone distributions from space, *Nature*, 392(6672), pp.168-171, 1998.

2057

2058

2059 [Myhre, G., Aas, W., Cherian, R., Collins, W., Faluvegi, G., Flanner, M., Forster, P., Hodnebrog,](#)  
2060 [Ø., Klimont, Z., Lund, M.T. and Mülmenstädt, J.: Multi-model simulations of aerosol and ozone](#)  
2061 [radiative forcing due to anthropogenic emission changes during the period 1990–2015.](#)  
2062 [Atmospheric Chemistry and Physics, 17\(4\), pp.2709-2720, 2017.](#)

2063

2064 Naja, M., C Mallik, T. Sarangi, V Sheel, S. Lal, SO<sub>2</sub> measurements at a high altitude site in the  
2065 central [Himalayas](#)~~Himalayas~~: Role of regional transport, *Atmospheric Environment*,  
2066 doi:10.1016/j.atmosenv.2014.08.031, 2014.

2067

2068 Naja M., Piyush Bhardwaj, N. Singh, Phani Kumar, R. Kumar, N. Ojha, Ram Sagar, S. K.  
2069 Satheesh, K. Krishna Moorthy and V. R. Kotamarthi: High-frequency vertical profiling of  
2070 meteorological parameters using AMF1 facility during RAWEX–GVAX at ARIES, Nainital,  
2071 *Current Science*, vol 111, issue 1, 2016.

2072

2073 Nalli, N.R., Barnet, C.D., Reale, A., Tobin, D., Gambacorta, A., Maddy, E.S., Joseph, E., Sun, B.,  
2074 Borg, L., Mollner, A.K. and Morris, V.R.: Validation of satellite sounder environmental data

2098 records: Application to the Cross-track Infrared Microwave Sounder Suite, J. Geophys. Res.  
2099 Atmos., 118(24), pp.13-628, 2013.

2100

2101 Nalli, N.R., Gambacorta, A., Liu, Q., Tan, C., Iturbide-Sanchez, F., Barnet, C.D., Joseph, E.,  
2102 Morris, V.R., Oyola, M. and Smith, J.W.: Validation of Atmospheric Profile Retrievals from the  
2103 SNPP NOAA-Unique Combined Atmospheric Processing System. Part 2: Ozone, IEEE  
2104 Transactions on Geoscience and Remote Sensing, 56(1), pp.598-607, 2017.

2105

~~2106 Ojha, N., Naja, M., Sarangi, T., Kumar, R., Bhardwaj, P., Lal, S., Venkataramani, S., Sagar, R.,  
2107 Kumar, A. and Chandola, H.C.: On the processes influencing the vertical distribution of ozone  
2108 over the central Himalayas: Analysis of yearlong ozonesonde observations, Atmospheric  
2109 Environment, 88, pp.201-211, 2014.~~

2110

2111 Nassar, R., Logan, J.A., Worden, H.M., Megretskaia, I.A., Bowman, K.W., Osterman, G.B.,  
2112 Thompson, A.M., Tarasick, D.W., Austin, S., Claude, H. and Dubey, M.K. Validation of  
2113 Tropospheric Emission Spectrometer (TES) nadir ozone profiles using ozonesonde measurements.  
2114 Journal of Geophysical Research: Atmospheres, 113(D15), 2008.

2115

2116 Ojha, N., Naja, M., Sarangi, T., Kumar, R., Bhardwaj, P., Lal, S., Venkataramani, S., Sagar, R.,  
2117 Kumar, A. and Chandola, H.C.: On the processes influencing the vertical distribution of ozone  
2118 over the central Himalayas: Analysis of yearlong ozonesonde observations, Atmospheric  
2119 Environment, 88, pp.201-211, 2014.

2120

- 2143 Pagano, T.S., Aumann, H.H., Hagan, D.E. and Overoye, K.: Prelaunch and in-flight radiometric  
2144 calibration of the Atmospheric Infrared Sounder (AIRS), IEEE transactions on geoscience and  
2145 remote sensing, 41(2), pp.265-273, 2003.
- 2146
- 2147 Pierce, R.B., Al-Saadi, J., Kittaka, C., Schaack, T., Lenzen, A., Bowman, K., Szykman, J., Soja,  
2148 A., Ryerson, T., Thompson, A.M. and Bhartia, P.: Impacts of background ozone production on  
2149 Houston and Dallas, Texas, air quality during the Second Texas Air Quality Study field mission,  
2150 J. Geophys. Res. Atmos., 114(D7), 2009.
- 2151
- 2152 Pittman, J.V., Pan, L.L., Wei, J.C., Irion, F.W., Liu, X., Maddy, E.S., Barnet, C.D., Chance, K.  
2153 and Gao, R.S.: Evaluation of AIRS, IASI, and OMI ozone profile retrievals in the extratropical  
2154 tropopause region using in situ aircraft measurements, J. Geophys. Res. Atmos., 114(D24), 2009.
- 2155
- 2156 Ramaswamy, V., Boucher, O., Haigh, J., Hauglustaine, D., Haywood, J., Myhre, G., Nakajima,  
2157 T., Shi, G.Y. and Solomon, S.: Radiative forcing of climate change. Climate change 2001: the  
2158 scientific basis. Contribution of working group I to the third assessment report of the  
2159 intergovernmental panel on climate change. DJ Griggs, M Noguer, PJ van der Linden, X Dai, K  
2160 Maskell and CA Johnson (Cambridge: Cambridge University Press) pp, 350, p.416, 2001.
- 2161
- 2162 Rawat, P., Naja, M., Thapliyal, P.K., Srivastava, S., Bhardwaj, P., Kumar, R., Bhattacharjee, S.,  
2163 Venkatramani, S., Tiwari, S.N. and Lal, S.: Assessment of vertical ozone profiles from INSAT-  
2164 3D sounder over the Central Himalaya. Current Science, 119(7), p.1113, 2020.

- 2188 Rawat, P. and Naja, M.: Remote sensing study of ozone, NO<sub>2</sub>, and CO: some contrary effects of  
2189 SARS-CoV-2 lockdown over India. *Environ Sci Pollut Res*, [https://doi.org/10.1007/s11356-021-](https://doi.org/10.1007/s11356-021-17441-2)  
2190 17441-2, 2021.
- 2191 Rodgers, C.D., 1976. Retrieval of atmospheric temperature and composition from remote  
2192 measurements of thermal radiation. *Reviews of Geophysics*, 14(4), pp.609-624.  
2193
- 2194 Rodgers, C.D., 1990. Characterization and error analysis of profiles retrieved from remote  
2195 sounding measurements. *Journal of Geophysical Research: Atmospheres*, 95(D5), pp.5587-5595.  
2196
- 2197 Rodgers, C.D. and Connor, B.J., 2003. Intercomparison of remote sounding instruments. *Journal*  
2198 *of Geophysical Research: Atmospheres*, 108(D3).  
2199
- 2200 Sarangi T., M. Naja, N. Ojha, R. Kumar, S. Lal, S. Venkataramani, A. Kumar, R. Sagar and H. C.  
2201 Chandola: First simultaneous measurements of ozone, CO and NO<sub>y</sub> at a high altitude regional  
2202 representative site in the central Himalayas, *J. Geophys. Res.*, 119, doi:10.1002/2013JD020631,  
2203 2014.  
2204
- 2205 Schwartz, M., Froidevaux, L., Livesey, N. and Read, W.: MLS/Aura Level 2 Ozone (O<sub>3</sub>) Mixing  
2206 Ratio V004, Greenbelt, MD, USA, Goddard Earth Sciences Data and Information Services Center  
2207 (GES DISC), 10.5067/Aura/MLS/DATA2017, 2015.  
2208
- 2209 Shindell, D., Kuylenstierna, J.C., Vignati, E., van Dingenen, R., Amann, M., Klimont, Z.,  
2210 Anenberg, S.C., Muller, N., Janssens-Maenhout, G., Raes, F. and Schwartz, J.: Simultaneously



2233 mitigating near-term climate change and improving human health and food security, *Science*,  
2234 335(6065), pp.183-189, 2012.

2235

2236 Smit, H.G., Straeter, W., Johnson, B.J., Oltmans, S.J., Davies, J., Tarasick, D.W., Hoegger, B.,  
2237 Stubi, R., Schmidlin, F.J., Northam, T. and Thompson, A.M.: Assessment of the performance of  
2238 ECC-ozonesondes under quasi-flight conditions in the environmental simulation chamber:  
2239 Insights from the Juelich Ozone Sonde Intercomparison Experiment (JOSIE), *Journal of*  
2240 *Geophysical Research: Atmospheres*, 112(D19), 2007.

2241

2242 Srivastava S., Manish Naja, V. Thouret: Influences of regional pollution and long range transport  
2243 over Hyderabad using ozone data from MOZAIC, *Atmospheric Environment*, 117, pp.135-146,  
2244 2015.

2245

2246 Stevenson, D.S., Young, P.J., Naik, V., Lamarque, J.F., Shindell, D.T., Voulgarakis, A., Skeie,  
2247 R.B., Dalsoren, S.B., Myhre, G., Berntsen, T.K. and Folberth, G.A.: Tropospheric ozone changes,  
2248 radiative forcing and attribution to emissions in the Atmospheric Chemistry and Climate Model  
2249 Intercomparison Project (ACCMIP), *Atmos. Chem. Phys.*, 13(6), pp.3063-3085, 2013.

2250

2251 Susskind, J., Barnett, C.D. and Blaisdell, J.M.: Retrieval of atmospheric and surface parameters  
2252 from AIRS/AMSU/HSB data in the presence of clouds, *IEEE Transactions on Geoscience and*  
2253 *Remote Sensing*, 41(2), pp.390-409, 2003.

2254

2279 Susskind, J., Barnett, C., Blaisdell, J., Iredell, L., Keita, F., Kouvaris, L., Molnar, G. and Chahine,  
2280 M.: Accuracy of geophysical parameters derived from Atmospheric Infrared Sounder/Advanced  
2281 Microwave Sounding Unit as a function of fractional cloud cover, *J. Geophys. Res. Atmos.*,  
2282 111(D9), 2006.

2283  
2284 [Tarasick, D., Galbally, I.E., Cooper, O.R., Schultz, M.G., Ancellet, G., Leblanc, T., Wallington,](#)  
2285 [T.J., Ziemke, J., Liu, X., Steinbacher, M. and Staehelin, J.: Tropospheric Ozone Assessment](#)  
2286 [Report: Tropospheric ozone from 1877 to 2016, observed levels, trends and uncertainties.](#)  
2287 [Elementa: Science of the Anthropocene, 7, 2019.](#)

2288  
2289 [Thornhill, G.D., Collins, W.J., Kramer, R.J., Olivié, D., Skeie, R.B., O'Connor, F.M., Abraham,](#)  
2290 [N.L., Checa-Garcia, R., Bauer, S.E., Deushi, M. and Emmons, L.K.: Effective radiative forcing](#)  
2291 [from emissions of reactive gases and aerosols—a multi-model comparison. \*Atmospheric Chemistry\*](#)  
2292 [and \*Physics\*, 21\(2\), pp.853-874, 2021.](#)

2293  
2294 Veefkind, J.P., de Haan, J.F., Brinksma, E.J., Kroon, M. and Levelt, P.F.: Total ozone from the  
2295 Ozone Monitoring Instrument (OMI) using the DOAS technique, *IEEE transactions on geoscience*  
2296 *and remote sensing*, 44(5), pp.1239-1244, 2006.

2297  
2298 Verstraeten, W. W., Boersma, K. F., Zörner, J., Allaart, M. A. F., Bowman, K. W., and Worden,  
2299 J. R.: Validation of six years of TES tropospheric ozone retrievals with ozonesonde measurements:  
2300 implications for spatial patterns and temporal stability in the bias, *Atmos. Meas. Tech.*, 6, 1413–  
2301 1423, <https://doi.org/10.5194/amt-6-1413-2013>, 2013.

2302

2324 Wang, W.C., Zhuang, Y.C. and Bojkov, R.D.: Climate implications of observed changes in ozone  
2325 vertical distributions at middle and high latitudes of the Northern Hemisphere, Geophysical  
2326 research letters, 20(15), pp.1567-1570, 1993.

2327

2328 Wang, B., R. Wu, K.-M. Lau: Interannual variability of Asian summer monsoon: Contrast between  
2329 the Indian and western North Pacific-East Asian monsoons. J. Climate, 14, 4073-4090, 2001.

2330

2331 Wang, H.R., Damadeo, R., Flittner, D., Kramarova, N., Taha, G., Davis, S., Thompson, A.M.,  
2332 Strahan, S., Wang, Y., Froidevaux, L. and Degenstein, D.: Validation of SAGE III/ISS Solar  
2333 Occultation Ozone Products With Correlative Satellite and Ground-Based Measurements. Journal  
2334 of Geophysical Research: Atmospheres, 125(11), p.e2020JD032430, 2020.

2335

2336 Wang, W., Cheng, T., van der A, R.J., de Laat, J. and Williams, J.E.: Verification of the  
2337 Atmospheric Infrared Sounder (AIRS) and the Microwave Limb Sounder (MLS) ozone algorithms  
2338 based on retrieved daytime and night-time ozone, Atmos. Meas. Tech., 14(2), pp.1673-1687, 2021.

2339

2340 Zhang, L., Jacob, D.J., Liu, X., Logan, J.A., Chance, K., Eldering, A. and Bojkov, B.R.:  
2341 Intercomparison methods for satellite measurements of atmospheric composition: application to  
2342 tropospheric ozone from TES and OMI. Atmospheric Chemistry and Physics, 10(10), pp.4725-  
2343 4739, 2010.

2344

2369 Zhu, T., W. Lin, Y. Song, X. Cai, H. Zou, L. Kang, L. Zhou, and H. Akimoto: Downward transport  
2370 of ozone-rich air near Mt. Everest, *Geophys. Res. Lett.*, 33, L23809, doi:10.1029/2006GL027726,  
2371 2006.

2372

2373 Ziemke, J.R., Chandra, S. and Bhartia, P. K.: Two new methods for deriving tropospheric column  
2374 ozone from TOMS measurements: Assimilated UARS MLS/HALOE and convective-cloud  
2375 differential techniques, *J. Geophys. Res. Atmos.*, 103(D17), pp.22115-22127, 1998.

2376

2377 Ziemke, J.R., Chandra, S., Duncan, B.N., Froidevaux, L., Bhartia, P.K., Levelt, P.F. and Waters,  
2378 J.W.: Tropospheric ozone determined from Aura OMI and MLS: Evaluation of measurements and  
2379 comparison with the Global Modeling Initiative's Chemical Transport Model, *J. Geophys. Res.*  
2380 *Atmos.*, 111(D19), 2006.

2381

2382

2383

2384

2385

2386

2387

2388

2389

2390

2391

2392

2407 [Zhang, R., Wang, H., Qian, Y., Rasch, P.J., Easter, R.C., Ma, P.L., Singh, B., Huang, J. and Fu,](#)  
 2408 [Q.: Quantifying sources, transport, deposition, and radiative forcing of black carbon over the](#)  
 2409 [Himalayas and Tibetan Plateau. Atmospheric Chemistry and Physics, 15\(11\), pp.6205-6223, 2015.](#)

2410

2411

2412

2413

2414

2415

2416

2417 **Table 1.** The mean values and corresponding standard errors of ozone mixing ratio (ppbv) from  
 2418 ozonesonde, ozonesonde(AK) and AIRS over Nainital at six pressure levels and during winter,  
 2419 spring, summer-monsoon, autumn are given. The number of ozonesonde flights during four  
 2420 seasons are mentioned in the bracket.

Pressure levels		706 (hPa)	496 (hPa)	300 (hPa)	103 (hPa)	29 (hPa)	14.4 (hPa)
Winter (61)	ozonesonde	55.1±0.9	54.4±0.7	69.5±2.8	238.8±15.0	4569.3±67.8	7620.6±140.1
	ozonesonde (AK)	48.6±0.4	55.9±0.6	70.4±1.8	187.3±3.6	5249.1±78.8	8214.9±105.7
	AIRS	46.5±0.3	52.2±0.6	68.7±1.2	354.4±8.4	4428.2±55.8	6616.4±56.0
Spring (72)	ozonesonde	71.6±1.8	70.2±1.5	81.5±2.8	223.9±12.7	4747.0±42.6	8242.3±101.6
	ozonesonde (AK)	58.7±0.7	69.1±1.1	80.3±1.4	221.8±3.6	5137.8±63.4	8784.4±96.6
	AIRS	55.3±0.4	60.7±0.7	78.6±1.0	389.2±6.0	4687.4±38.2	7852.4±97.0

Summer- monsoon (55)	ozonesonde	53.0±2.7	65.1±2.7	82.1±2.5	138.6±3.4	4642.9±26.4	8493.6±91.1
	ozonesonde (AK)	44.1±1.2	62.3±1.7	68.7±1.7	224.3±3.4	5271.3±44.6	9233.8±72.4
	AIRS	48.8±0.5	57.5±0.5	63.6±0.6	267.4±5.5	4710.0±48.2	8333.1±82.5
Autumn (54)	ozonesonde	53.0±1.1	63.8±1.6	72.7±1.6	144.6±6.2	4439.3±28.2	8613.7±77.5
	ozonesonde (AK)	50.4±0.5	61.0±0.8	64.1±0.9	169.0±2.0	5086.3±38.7	9035.8±80.7
	AIRS	46.0±0.3	51.3±0.4	56.9±30.5	241.8±3.6	4635.4±43.9	7984.9±97.6

2425 **Table 2.** Coefficient of determination ( $r^2$ ) of three IR satellite sensors (AIRS, IASI and CrIS) ozone  
 2426 retrieval in five broad layers with respect to ozonesonde observations.

	Coefficient of determination ( $r^2$ )		
	AIRS	IASI	CrIS
600 - 800 hPa	0.52	0.34	0.09
300 - 600 hPa	0.44	0.31	0.22
100 - 300 hPa	0.45	0.44	0.45
50-100 hPa	0.87	0.76	0.82
10 - 50 hPa	0.94	0.80	0.94

2427

2428

2438 **Table 3.** Total column ozone (TCO) differences in DU between AIRS, OMI and ozonesonde,  
 2439 during twelve months.

TCO Diff. (DU)	Jan	Feb	Mar	Apr	May	Jun	Jul	Aug	Sep	Oct	Nov	Dec
AIRS-OMI	-3.9	2.2	-1.8	13.2	16.7	18	-2.2	17.2	22.1	13.2	0.0	-2.7
AIRS-ozonesonde	-2.1	3.5	6.0	8.1	19.4	11.8	-2.3	22.3	21.6	15.0	5.6	5.2

2440

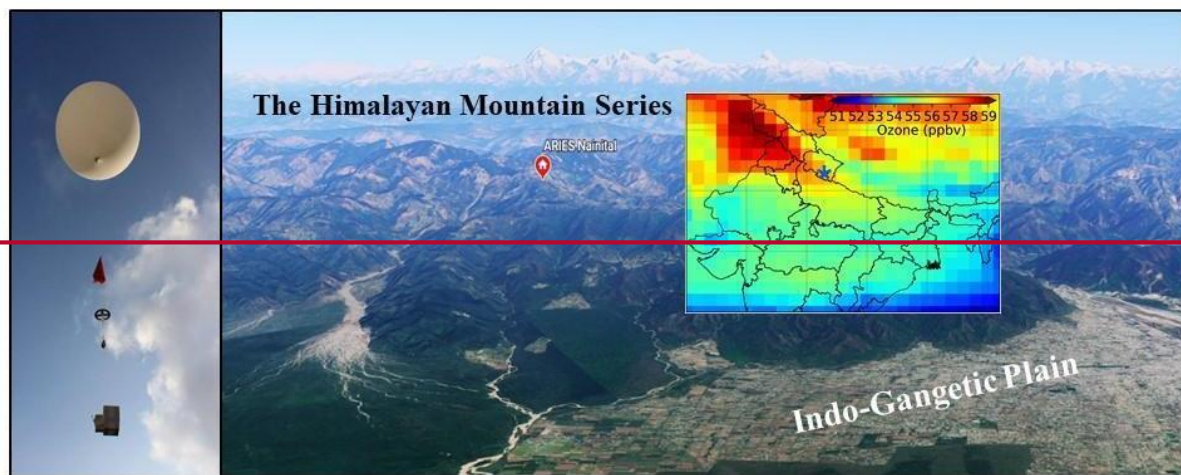
2441

2442

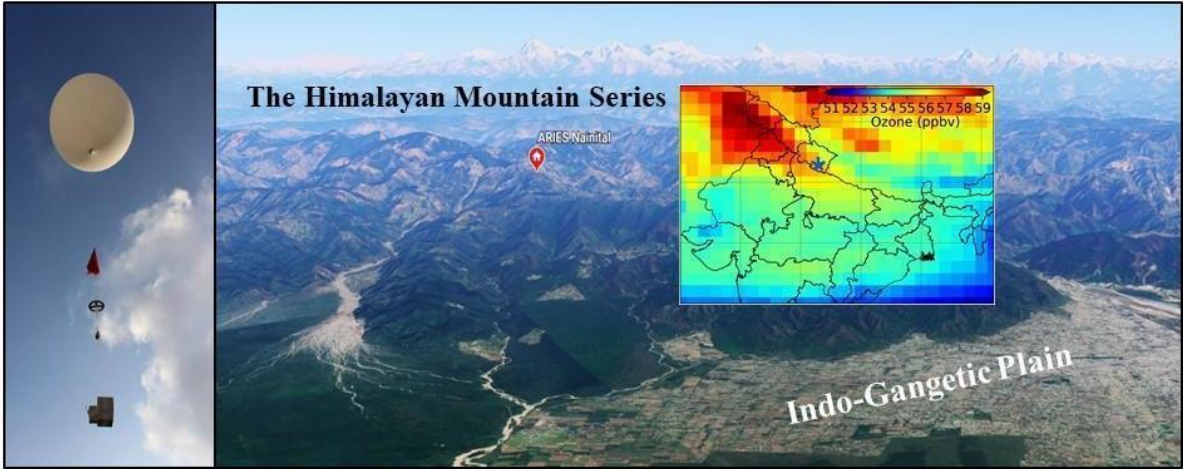
2443

2444

2445



2446



2459

2460 **Figure 1.** Location (red color circle) of the balloon launching site (Map from Google Earth, 2021)  
2461 situated in the Aryabhata Research Institute of Observational Sciences (ARIES) (29.4° N, 79.5°  
2462 E, and 1793 m elevation), Nainital in the central Himalaya. The spatial distribution of ozone  
2463 (AIRS) at 500 hPa is also shown over northern India and the location of the site is marked with a  
2464 blue star. A photo of balloon, together with parachute, unwinder, ozonesonde along with GPS-  
2465 radiosonde above the observation site is also shown at the left.

2466

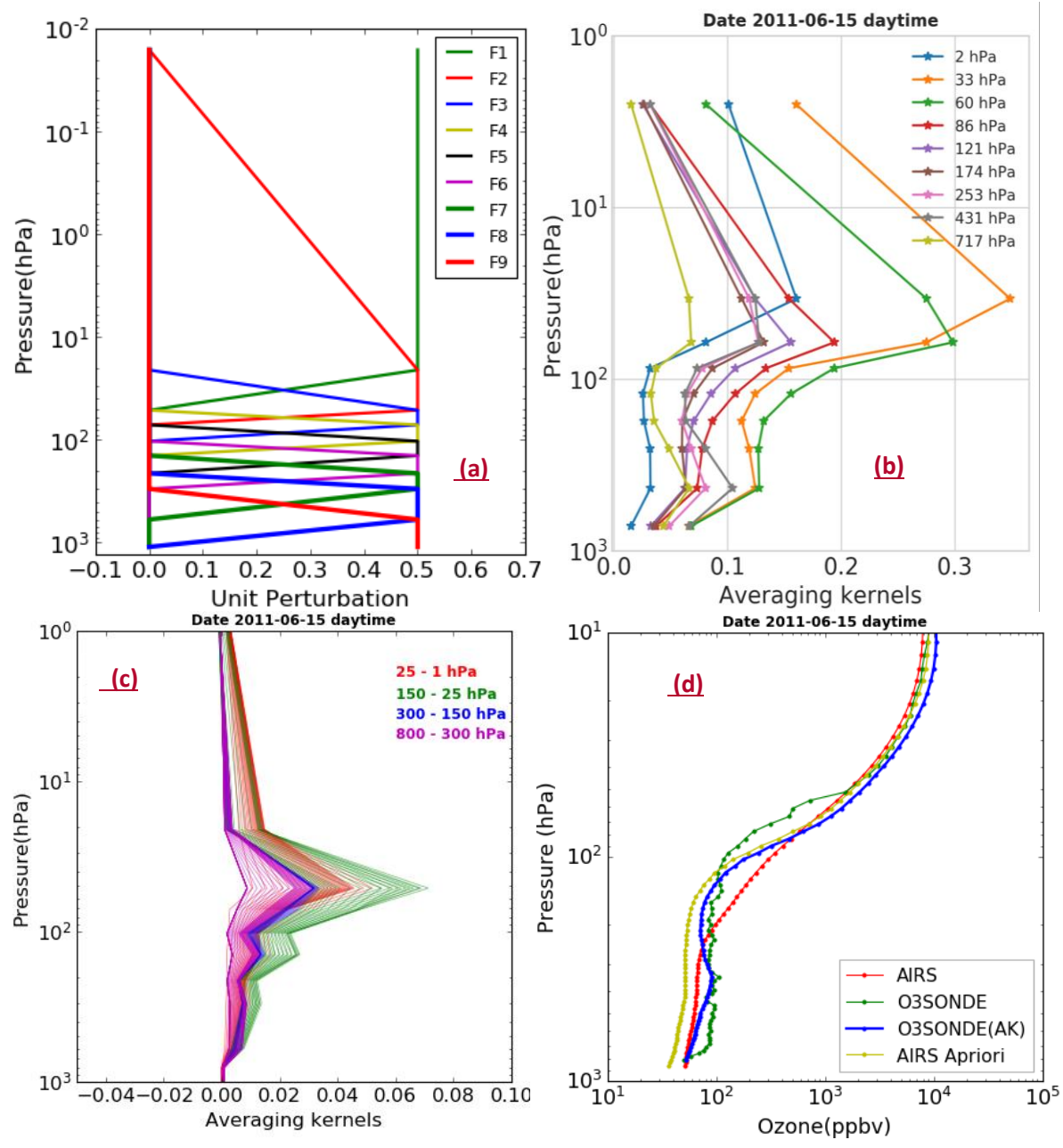
2467

2468

2469

2470



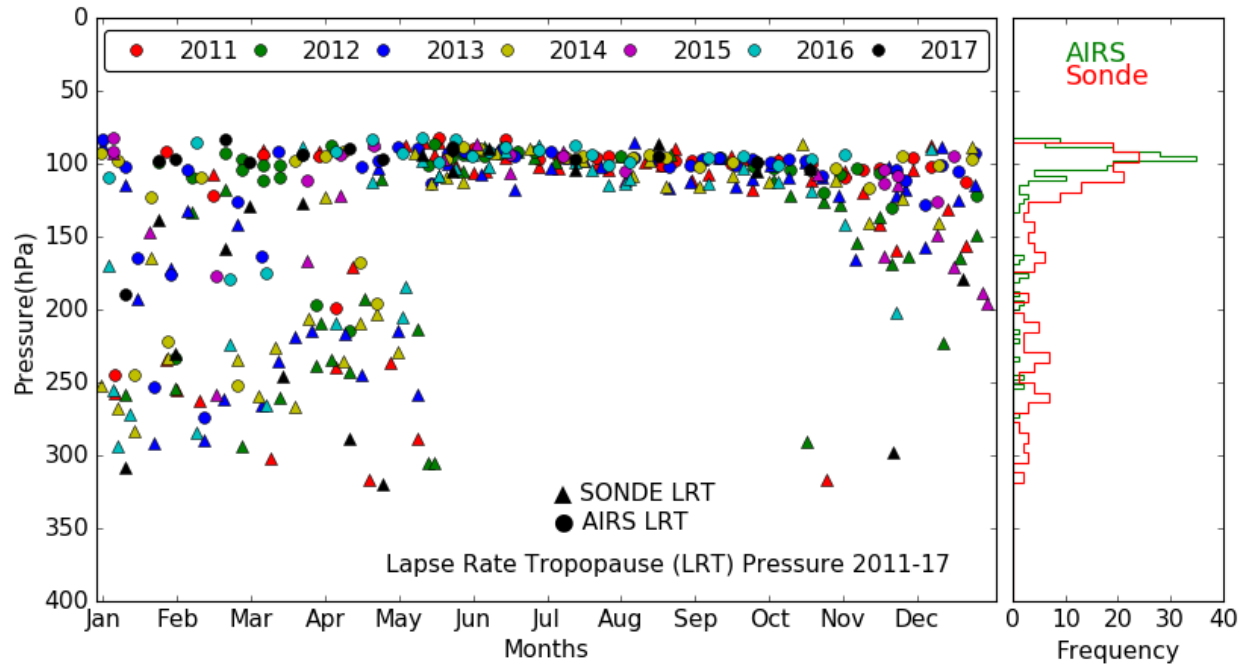


2478

2479  
2480

2481  
2482  
2483  
2484

**Figure 2.** (a) Nine trapezoid functions used for ozone retrieval in AIRS-V6. (b) AIRS ozone averaging kernel matrix over Nainital at 9 levels vertical grid. (c) Calculated AIRS averaging kernel matrices at 100 RTA grids after applying the trapezoid function. (d) An example of ozone profiles using different data sets for 15 Jun 2011 over the observation site.



2498

2499 **Figure 3.** Lapse rate tropopause pressure monthly variation from balloon-borne and AIRS  
2500 observations and respective frequency distributions during 2011 - 2017.

2501

2502

2503

2504

2505

2506

2507

2508

2509

2510

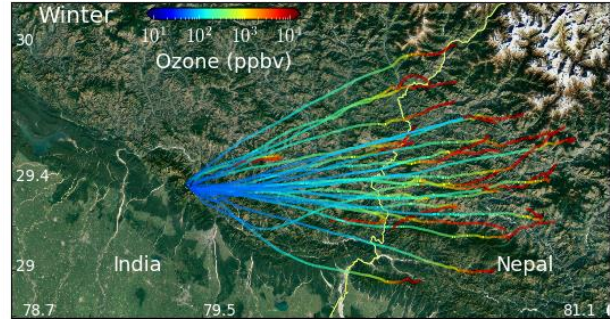
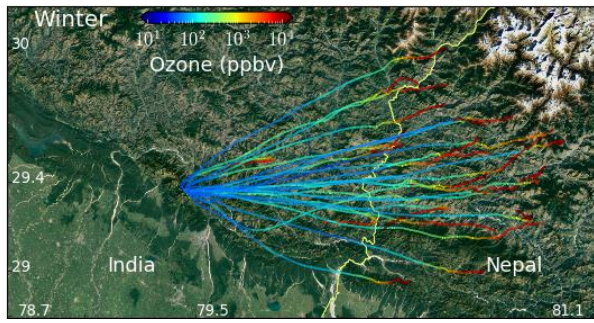


2523

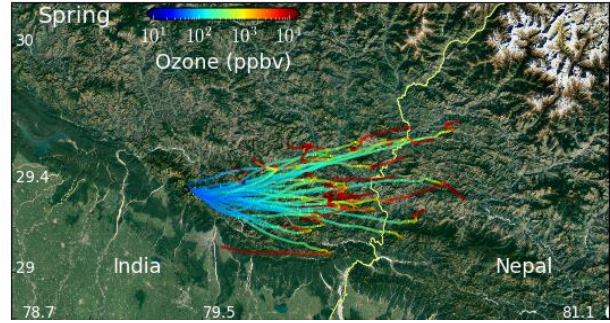
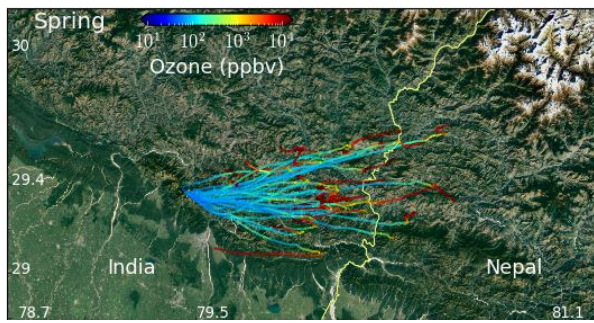
Ozonesonde

AIRS

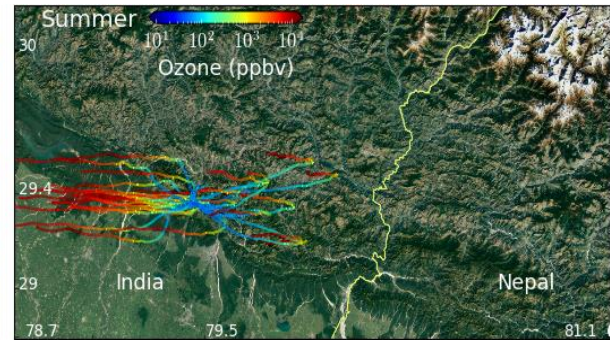
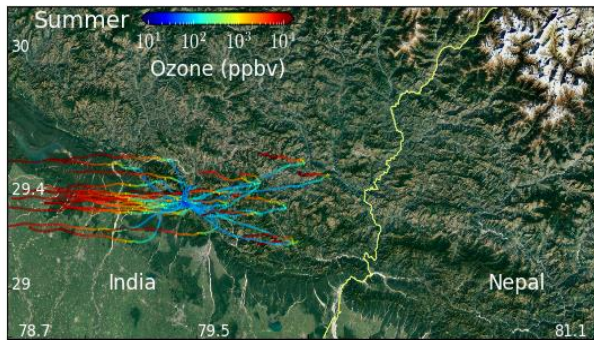
2524



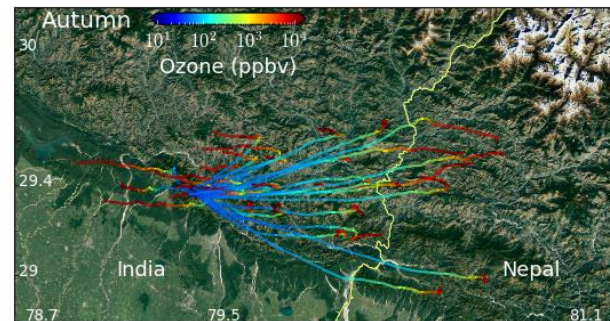
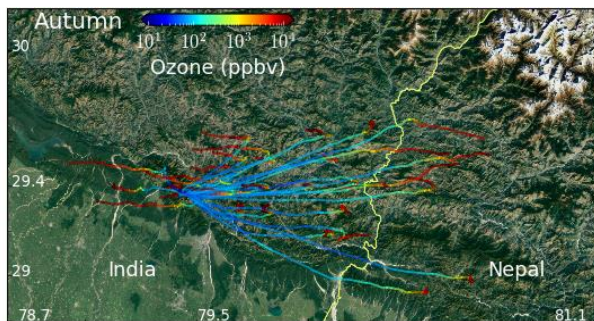
2525



2526



2527



2528

2529

2530

2531

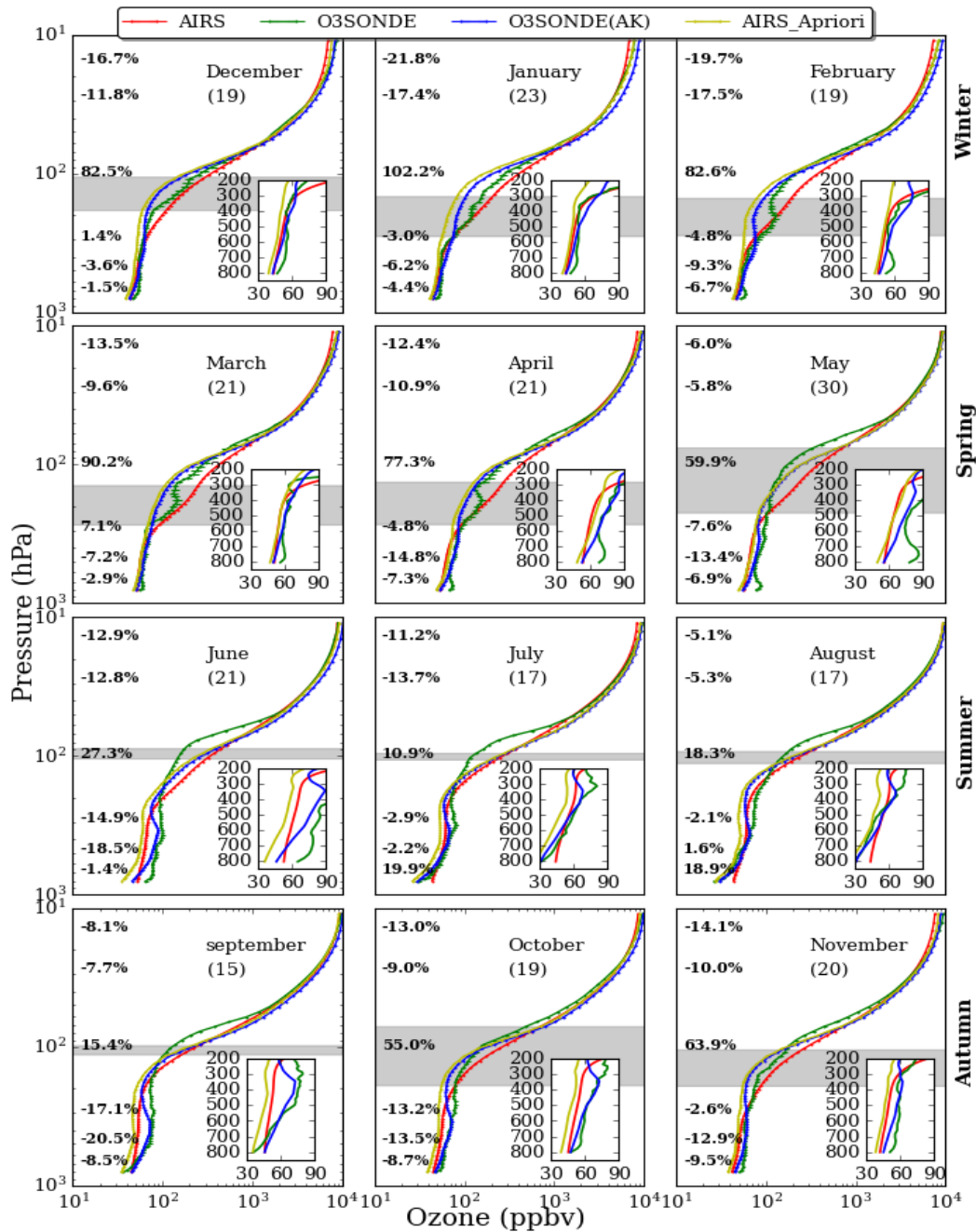
2532

2533

2534

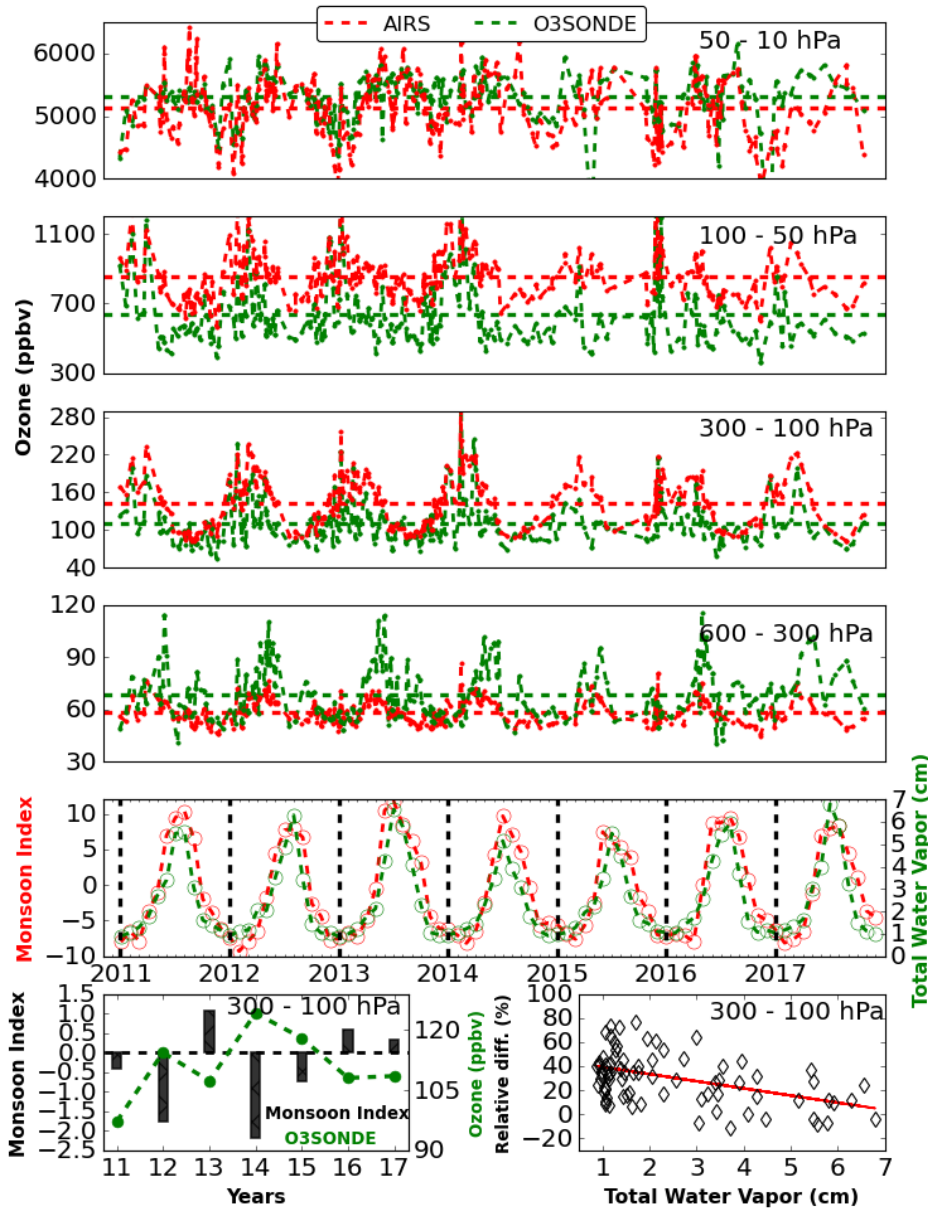
**Figure 4.** Spatial distribution of ozone using all ozone soundings (left) launched from ARIES, Nainital, India (India (Map from Google Earth, 2021), along with the balloon trajectories. Ozone spatial distribution from AIRS (right), following the balloon tracks, is also shown. It could be seen that the balloon reaches Nepal many times in the winter and autumn seasons.





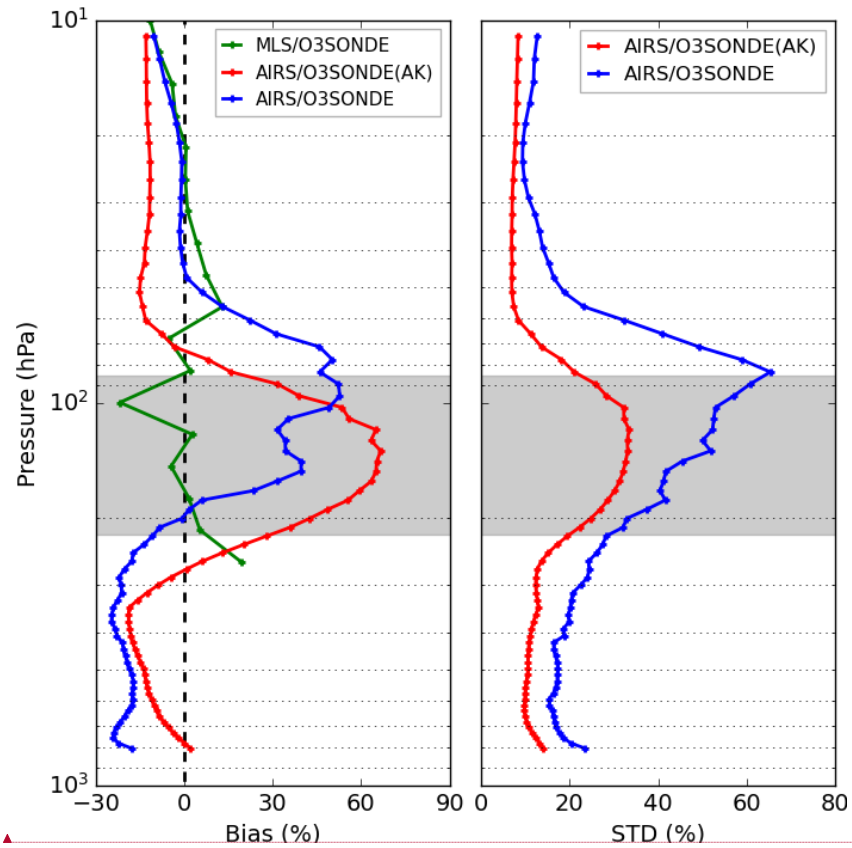
2542

2543 **Figure 5.** Monthly averaged (2011-2017) ozone profiles of ozonesonde, AIRS, ozonesonde(AK)  
 2544 and AIRS a-priori over Nainital in the central Himalaya. The percentage difference  $[(\text{AIRS} -$   
 2545  $\text{ozonesonde(AK)})/\text{ozonesonde(AK)}]*100$  at 706, 496, 300, 103, 29, and 14.4 hPa are also written  
 2546 at respective altitudes. The standard error corresponding to each profile is also shown with  
 2547 errorbars. The number of ozonesonde for different months is written in the bracket and grey shaded  
 2548 area shows the tropopause (mean $\pm$ sigma) from balloon-borne observations.



2560

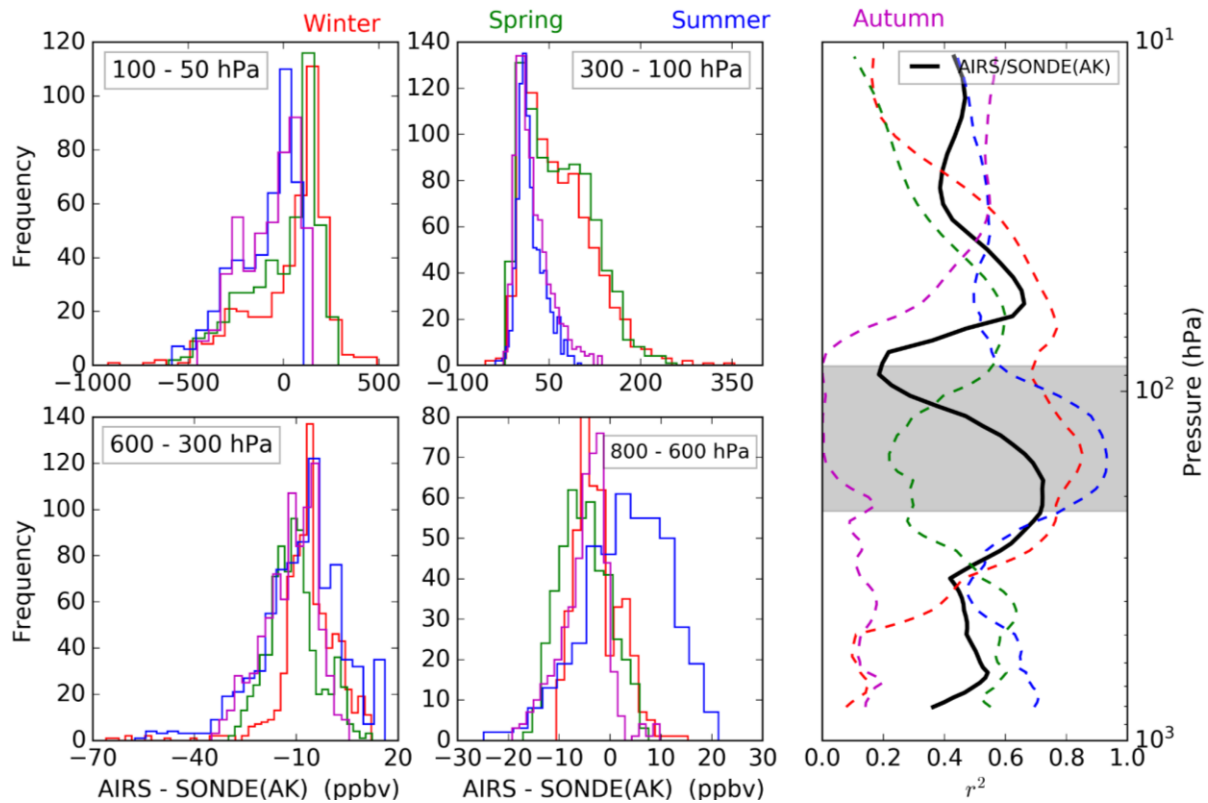
2561 **Figure 6.** Average variations in ozone mixing ratios at four defined layers, characterizing the  
 2562 middle stratosphere (50 - 10 hPa), the lower stratosphere (100 - 50 hPa), the upper troposphere  
 2563 (300 - 100 hPa), and the middle troposphere (600 - 300 hPa), respectively. The red and green dash  
 2564 horizontal lines show the average ozone mixing ratios in the defined layers from AIRS and  
 2565 ozonesonde, respectively for, from 2011 to 2017. The monthly variation of the total column water  
 2566 vapor (cm) along with the monsoon index is also shown. The (left lower most) The yearly average  
 2567 ozone from ozonesonde and monsoon index (bar plot) for different years and (right lower most)  
 2568 scattered plot of ozone relative difference (%) [(AIRS-O3SONDE)/O3SONDE]\*100, with  
 2569 monsoon index and total water vapor in the upper troposphere (300 - 100 hPa) is also shown.  
 2570 at the bottom.



2578

2579 **Figure 7.** Statistical error analysis (Bias and standard deviation) of AIRS retrieved ozone with  
 2580 ozonesonde and ozonesonde (AK) for collocated data of seven years (2011 - 2017). The Bias  
 2581 between collocated data of MLS (261 hPa - 10 hPa) and ozonesonde over Nainital during 2011 -  
 2582 2017 is also shown with the green profile. The grey shaded area shows the tropopause region from  
 2583 balloon-borne radiosondes observations.

2584



2594

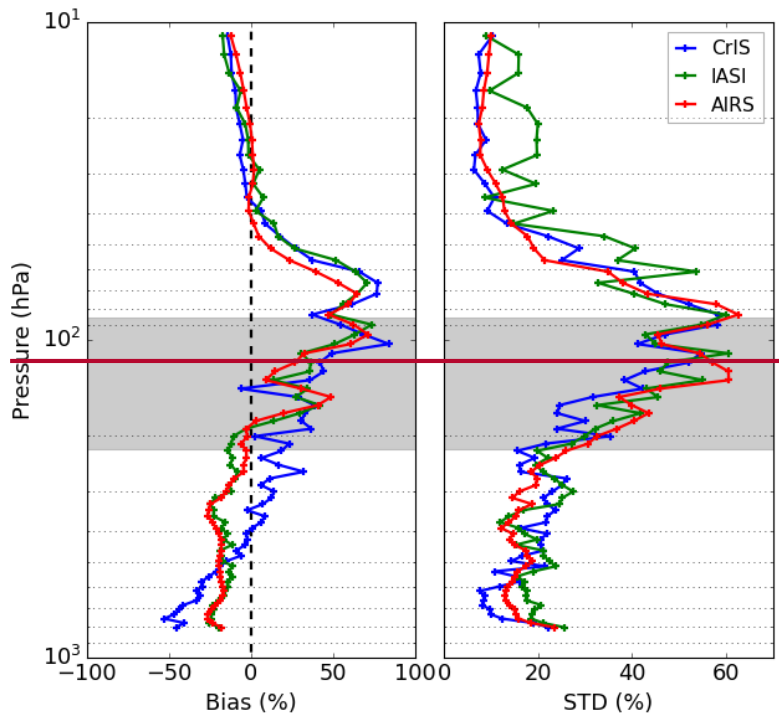
2595 **Figure 8.** Histogram difference between AIRS ozone and ozonesonde(AK) in the four defined  
 2596 layers. The average correlation profiles between AIRS ozone and ozonesonde(AK) are shown on  
 2597 the right during winter (red), spring (green), summer-monsoon (blue), and autumn (magenta). The  
 2598 black line is for the entire data set. The grey shaded area shows the tropopause region from balloon-  
 2599 borne radiosondes observations.

2600

2601

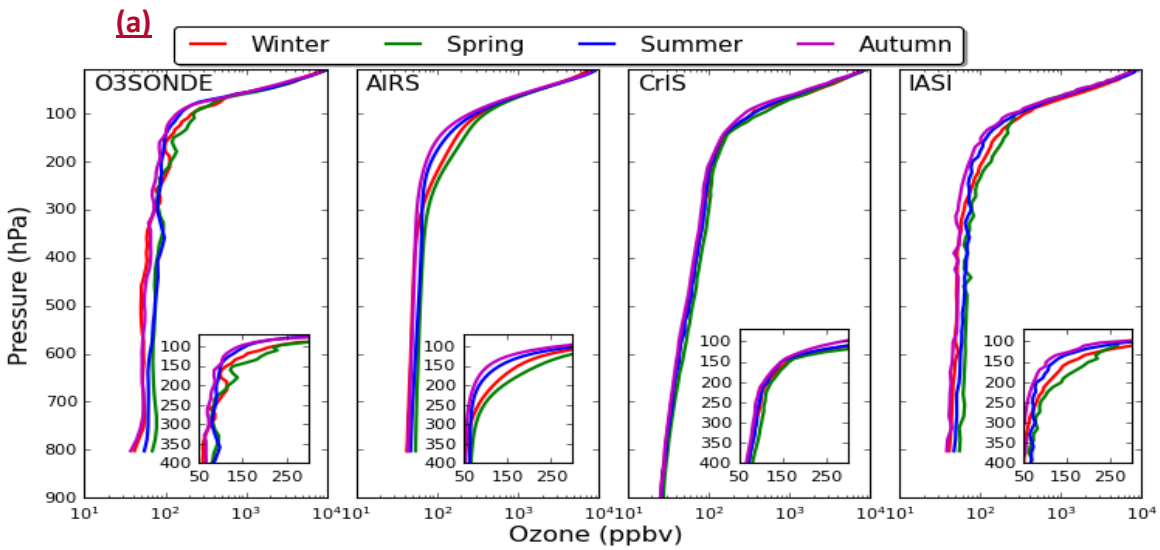
2602

(a)



2607

2608

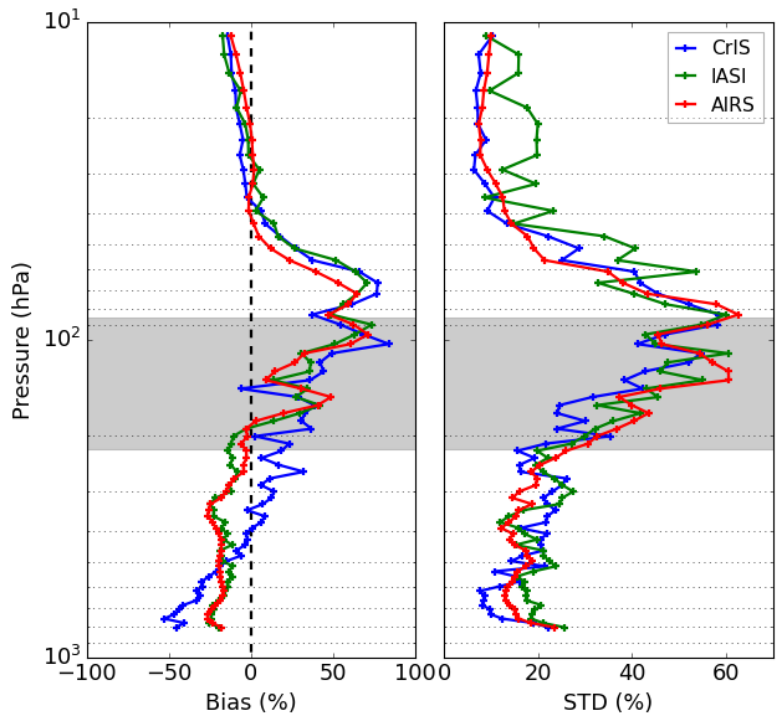


2609

2610

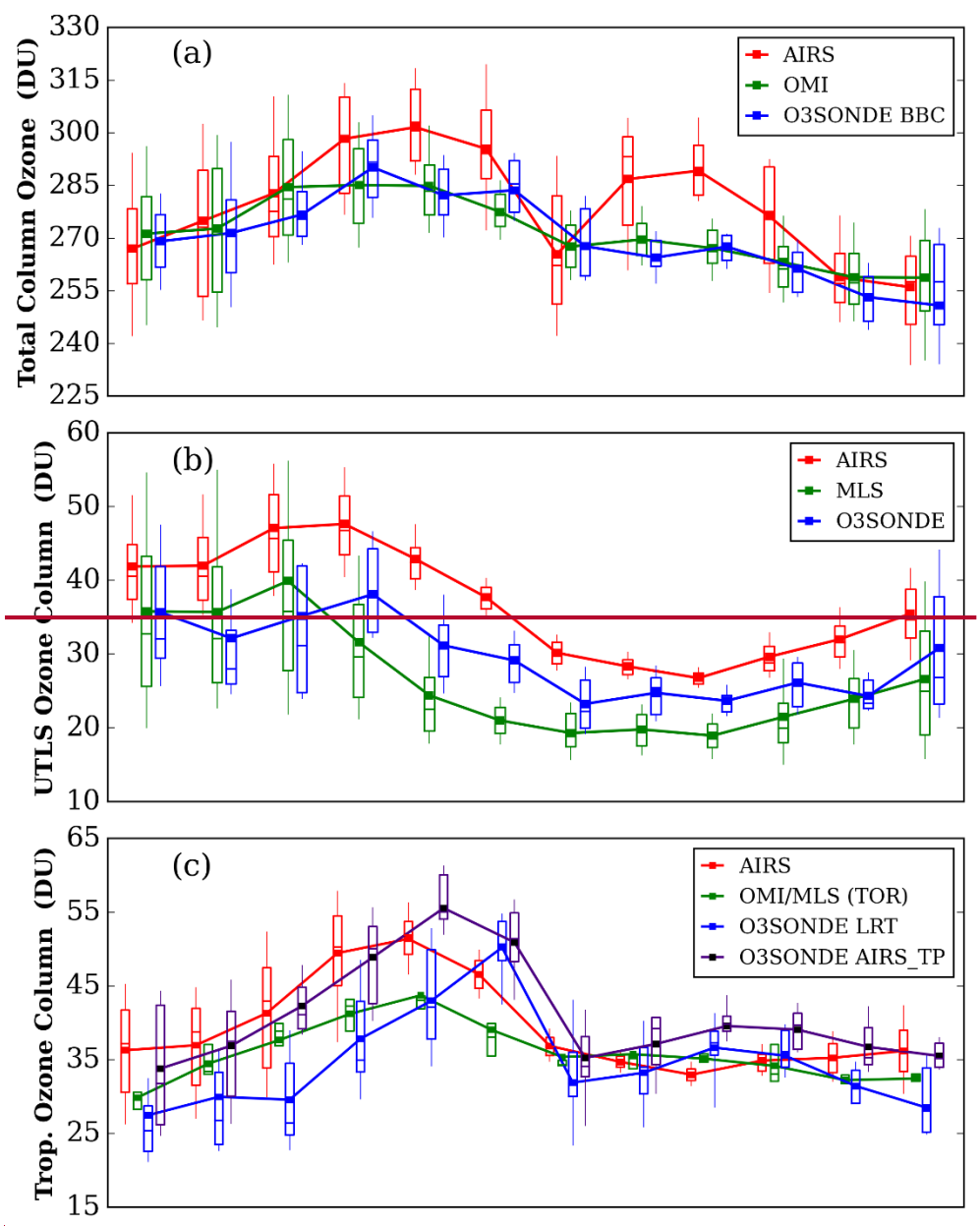
(b)



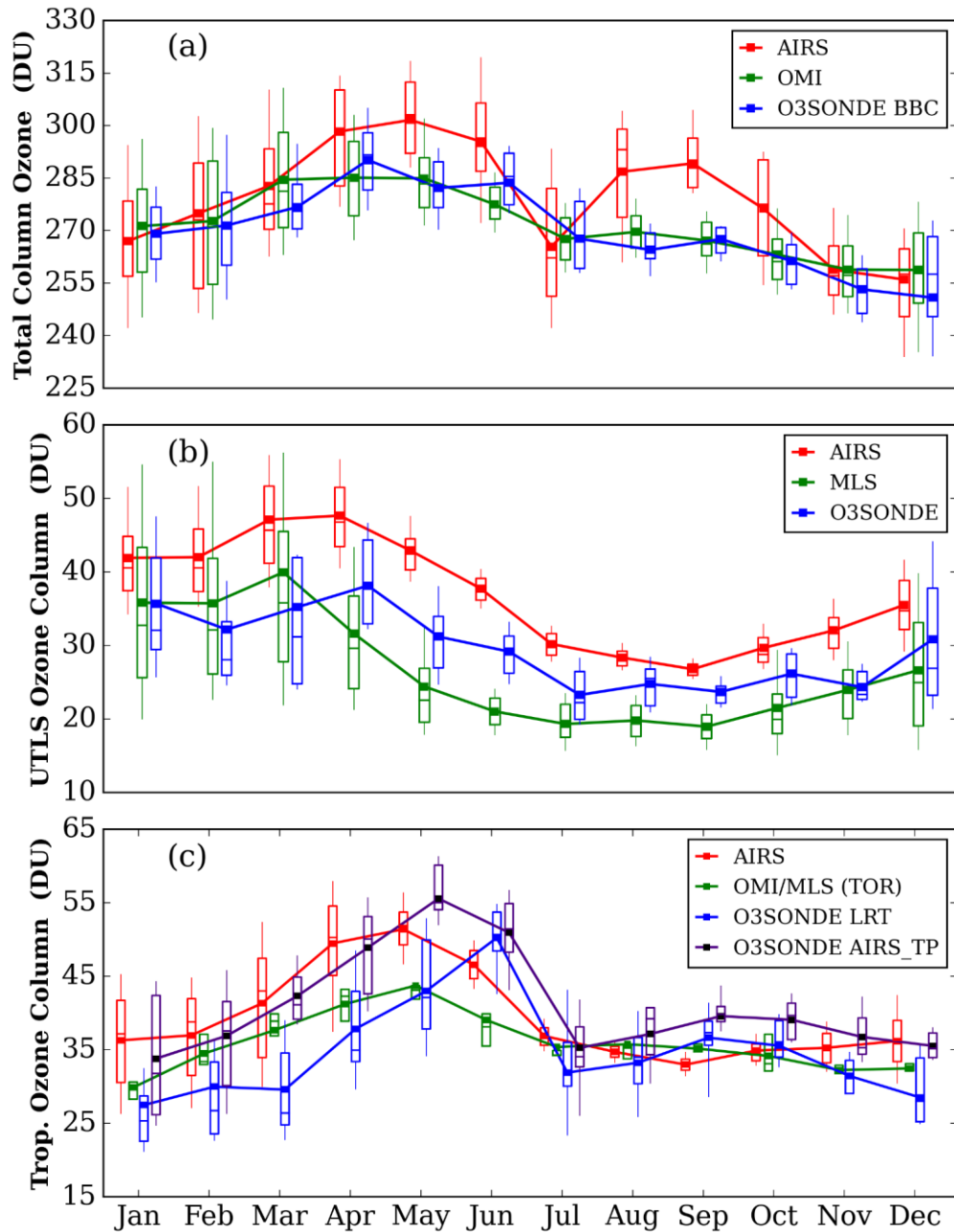


2617

2618 **Figure 9.** (a) Seasonal ozone profiles of three IR satellites (IASI, AIRS, and CrIS) for a smaller  
 2619 sample size (April 2014 to April 2015). The IASI and CrIS products are generated using the AIRS  
 2620 heritage algorithm (NOAA) and only zero quality flags (QC=0) of retrieval are used. (b) Statistical  
 2621 error analysis for the three IR satellites retrieved ozone without applying the averaging kernel  
 2622 information. The grey shaded area shows the tropopause region from balloon-borne observations.



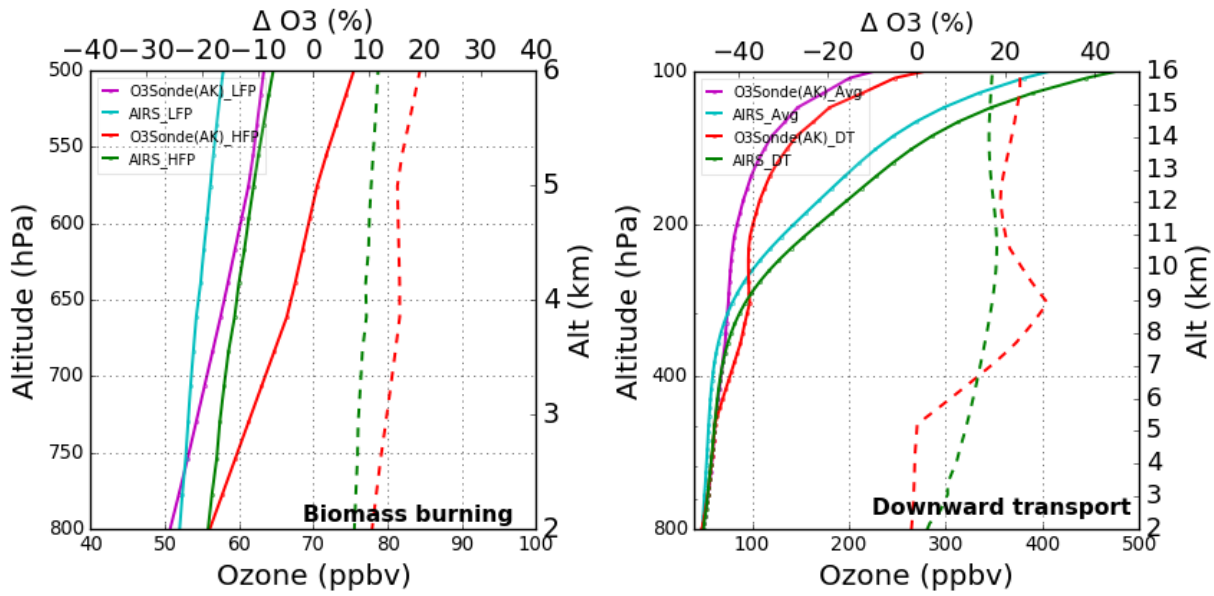
2624



2635

2636 **Figure 10.** (a) Monthly average variations of total column ozone (TCO) for AIRS, OMI, and  
 2637 ozonesonde (Balloon Burst Climatology) over the central Himalaya for the 2011-2017 period. (b)  
 2638 Monthly average variation of UTLS ozone column for AIRS, MLS, and ozonesonde, over the  
 2639 central Himalayas for the 2011-2017 period. (c) Monthly average variations of tropospheric ozone  
 2640 column of AIRS, OMI/MLS (Tropospheric Ozone Residual), and ozonesonde (LRT --- sonde lapse  
 2641 rate)); over the central Himalayas for the 2011-2017 period. The ozonesonde tropospheric ozone  
 2642 column is also shown using AIRS tropopause (AIRS\_TP). In the box plot, the lower and upper  
 2643 edges of the boxes represent the 25th and 75th percentiles. The whiskers below and above are 10th  
 2644 and 90th percentiles.

2656



2657

2658 **Figure 11. (a)** Vertical ozone profiles of AIRS ozone and ozonesonde(AK) during low fire period

2659 (LFP) and high fire period (HEP). The solid lines correspond to ozone profiles while the dotted

2660 lines show a percentage increase in ozonesonde (red) and AIRS (green) profiles during biomass

2661 burning events. (b) Vertical ozone profiles of AIRS ozone and ozonesonde(AK) during events of

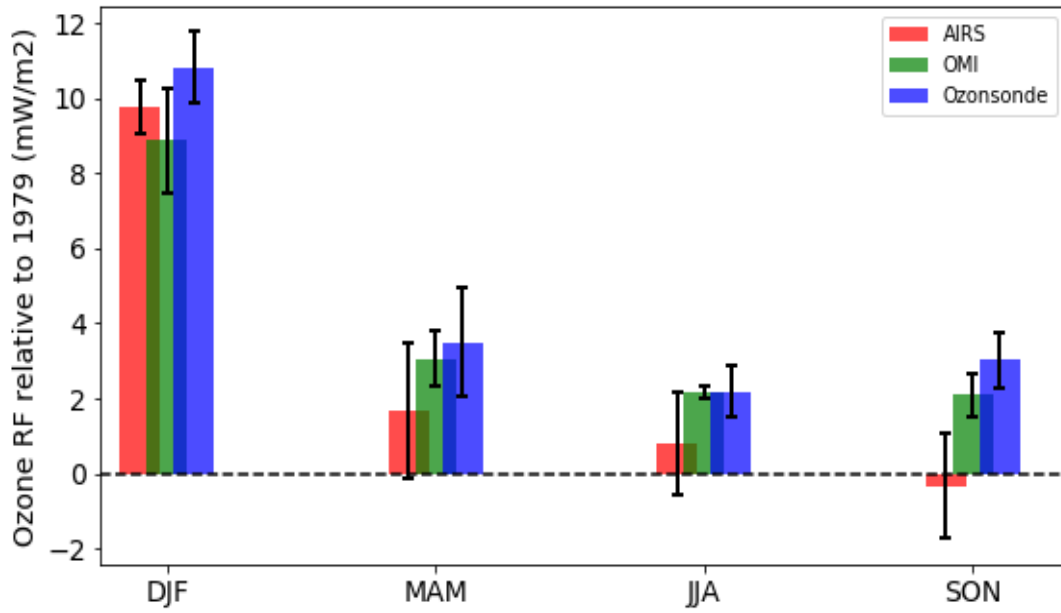
2662 downward transport. ~~Dotted~~The dotted line shows ozone enhancement during downward transport

2663 events.

2664

2665

2666



2672

2673 **Figure 12.** Seasonal average ozone UV radiative forcing (RF) relative to 1979 as calculated from  
 2674 ozonsonde, OMI, and AIRS total ozone data for the 2011 - 2017 period. Spreads correspond to  
 2675 one standard deviation.

2676